FINITE ELEMENT MODELING OF WELDED JOINTS USING EFFECTIVE NOTCH STRESS APPROACH

By

Md Nuruzzaman

A Thesis Submitted to the Faculty of Graduate Studies of

The University of Manitoba

In partial fulfilment of the requirements of the degree of

MASTER OF SCIENCE

Department of Mechanical Engineering

University of Manitoba

Winnipeg, Manitoba

Dedication

I would like to show my heartiest gratitude to my parents and my wife for the sacrifices they made for me and for always believing in me.

This thesis has contained the work from the following paper:

M. Nuruzzaman, C. Q. Wu, and O. Ojo, "*Modeling of Welding Joint using Effective Notch Stress Approach for Misalignment Analysis*", ASME 2015 International Mechanical Engineering Congress and Exposition, Houston, Texas 2015.

Abstract

Automotive structures contain hundreds of welds. Most of the time, failure occurs at the weld ends (weld toe or weld root). Thus, welds affect the structural integrity of an entire structure. Thus, the modeling of welded joints is very important from a design point of view. In this research, the primary aim is to develop a weld model to assess the structural integrity of welded joints based on stress analysis by using a finite element method (FEM) and through experimental validation. The stress distribution in welded joints mainly depends on the geometry, loading type and material properties. Therefore, it is greatly challenging to develop a weld model that can predict the behavior of stress distribution and weld stiffness in joints. There are several approaches for modeling welded structures by using FEM. However, the effective notch stress approach has been used for weld joint modeling in this research which is gaining in popularity in the automotive industry. The effective notch stress approach calculates the local stress at a notch (weld toe or root) assuming that there is linear-elastic material behavior. The finite element modeling and meshing of the welded joint using the effective notch stress approach has been performed following the recommendations of the International Institute of Welding (IIW) in this study. Parameter tuning of the weld model has been done to obtain the lowest validation error with the experimental results. The effective notch radius is chosen as the only tuning parameter in this weld model. Through this investigation, the weld model based on the effective notch stress has been experimentally validated for the first time through parameter tuning. Two different types of welded joints are investigated. Both types of joints are analyzed with a fine meshed 3D finite element model by using the effective notch stress approach. The FEM model of these two joints is validated with the experimental results. The calculated FEM results show a good agreement with the experimental results (obtained by using strain gages) for the ASTM model with an effective notch radius that is close to 0.2 mm. This reference radius is successfully used for the experimental validation of the misaligned ASTM specimens. This modeling technique is also validated with real world data of a bus window pillar. The model of the bus window pillar shows a close approximation with the experimental results. The experimental validation of the bus window pillar is not included in this thesis due to the confidentiality agreement.

Acknowledgements

I would like to gratefully thank my advisor, Dr. Christine Q. Wu, for her guidance in carrying out this work. I deeply appreciate her valuable time, assistance, patience and insight throughout the course of this research. This thesis would not have been possible without the opportunity, help and support that she has given me. Thank you, Dr. Wu.

Along with my advisor, I would also like to thank my co-advisor, Dr. Olanrewaju Ojo. I would like to express my appreciation for his valuable suggestions, comments and guidance which improved this work. As well, the guidance, supervision and help from Dr. Nan Wu are also greatly appreciated.

I would also like to thank my colleagues, Ms Tamrin Tanha, Mr. Anton Kuznetcov, and Mr. Khashayar Pejhan for their help in preparing for the tests.

Last but not least, I would like to thank my parents and friends for their significant support. Specifically, I would like to thank my wife for her inspiration, without which I could not have achieved my goals.

Table of Contents

List of Figures

List of Tables

Abbreviations

FEM	Finite Element Method
FEA	Finite Element Analysis
FE	Finite Element
ASTM	American Society for Testing and Materials
RAM	Random Access Memory
LEFM	Linear Elastic Fracture Mechanics
E	Elasticity of Modulus
IIW	International Institute of Welding
DNV	Det Norska Veritas
SS	Stainless Steel
HAZ	Heat affected zone
MPC	Multi-Point Contraint
ADC	Analog-to-Digital Converter
DAQ	Data acquisition
ITC	Industrial Technology Centre
CAD	Computer Aided Design

Nomenclature

σ_{mem}	Membrane stress (MPa)
σ_{ben}	Bending stress (MPa)
σ_{hss}	Hot spot stress (MPa)
$\Delta\sigma_{hss}$	Hot spot stress range (MPa)
$\Delta\sigma_{eff}$	Effective notch stress range (MPa)
ρ_f	Fictitious radius (mm)
ρ	Real notch radius (mm)
s	Factor for stress multiaxiality and strength criterion
ρ^*	Substitute micro-structural length (mm)
2α	Notch opening angle (degree)
x	Distance from plate surface (mm)
V_r	Voltage ratio (mV/mV)
$V_{O(strained)}$	Output voltage for strained condition (mV)
$V_{O(unstrained)}$	Output voltage for unstrained condition (mV)
V_{ex}	Excitation voltage (mV)
ε_θ	Normal strain at any angle θ from the major principal axis
ε_a	Strain in Grid 1 of the strain gage (mm/mm)
ε_b	Strain in Grid 2 of the strain gage (mm/mm)
ε_c	Strain in Grid 3 of the strain gage (mm/mm)

ε_x	Strain in the direction perpendicular to the weld toe (mm/mm)
ε_y	Strain in the direction parallel to the weld toe (mm/mm)
γ_{xy}	Shear strain (mm/mm)
θ_p	Angle of principal direction (degree)
ε_1	Maximum principal strain (mm/mm)
ε_2	Minimum principal strain (mm/mm)
υ	Poisson's ratio
σ_1	Maximum principal stress (MPa)
σ_2	Minimum principal stress (MPa)
σ_{vm}	von-Mises stress (MPa)

Chapter 1 Introduction

1.1 Background Information

For any automotive structure, structural integrity is an extremely important characteristic for safety and functionality. According to [1], "Structural integrity is the quality of a component, a single structure, or a structure consisting of different components to hold together under a load, including its own weight, resists any type failure". The chassis of automotive structures requires hundreds of welds and more. However, residual stresses are induced onto the chassis structure due to welding. The strength of welded structures is considerably lower than that of un-welded structures made of the same metal. Stress raisers are therefore introduced into welded structures due to the geometric discontinuity caused by the welding process. Stress raisers are governed by many factors, such as the transition zone between the weld and base materials, the location of the welds in a plane and the quality of the welding. The homogeneity and microstructure of the base material also change resultant of the filler material used during welding. Therefore, welding creates high tensile residual stresses, thus reducing the strength of welded structures. Another problem with welded structures is that no weld is ideal. There are always some sorts of defect, such as inclusions, misalignment, etc. Even the introduction of automatic welding cannot overcome the problems related to welding. The resultant stress concentrations then have a detrimental effect on the strength of the welded joints. So, welded joints affect the structural integrity of an entire structure. The loss of the structural integrity of any automotive structure is a catastrophic failure, which can result in severe damage, injuries, monetary losses or even death [1].

Figure 1- 1- 1 Typical Skeleton of Bus Frame [2]

One of the more well-known and leading bus companies, the name of which will not be disclosed here, indicated that some of the welded joints of the window pillars on the frames of their buses are very vulnerable to failure. Actually, the joints failed earlier than the company expected, which caused a substantially large monetary loss in honoring their structural warranty. They have their own finite element model of the bus structure. In their model, they have considered a perfect connection between the cross beam and the main structure. However, they did not consider the presence of welds in their finite element model. The effect of welded joints on the chassis model was neglected during the analysis of the structural integrity of the chassis of the bus. Investigation of the structural integrity of the frames without considering the welds with

the use of FEM could mean large discrepancies and consequently would lead to inaccuracies in the predicted result. Therefore, I have developed a weld joint modeling technique by using finite element analysis (FEA). This modeling technique will be suitable for investigating the structural integrity of chassis models that contain welded joints with the use of FEA.

There are several approaches for modeling the welded structures using finite element method. These approaches are mainly two types: global approaches and local approaches. In the past decades, the increased application of finite element modeling introduced local approaches more and more in the design concept of welded structure. The hot spot stress approach is the first local approach which was used widely for modeling of the pressure vessels and welded tubular joints for long time. But the hot spot stress approach cannot calculate the stress at the critical areas of the welded joints accurately [3]–[7].

There are several approaches for modeling welded structures by using FEM. These approaches mainly comprise two types: global and local. In the past decades, local approaches during the design concept of welded structures have been increasingly used and applied in finite element modeling. The hot spot stress approach is the first local approach which is widely used for modeling pressure vessels and welded tubular joints. However, the hot spot stress approach cannot be used to accurately calculate the stress at the critical areas of welded joints [3]–[7].

The most recent local approach is the effective notch stress approach for modeling welded structures with the use of FEA. This modeling technique and its guidelines have been recently recommended by the International Institute of Welding (IIW) [6]. This approach can be used to

develop finite element models that assess the stress at the weld root as well as the weld toe. This most recent modeling approach for welded joints is based on the introduction of a so-called effective notch stress that occurs at the toe/ root of a weld. The notch stress in a welded joint is the sum of the local stress caused by both the geometrical irregularities and the local stress raiser, i.e. the weld itself. According to this concept, the geometry of the weld toe is replaced by a rounding or circular notch (fictitious notch) with a specific radius. The stress distribution around the weld toe can then be calculated with FE techniques [4], [6], [7]. Details of this modeling technique will be discussed in the chapter on the literature review.

This thesis mainly focuses on the effective notch stress approach based on weld-end modeling that takes into consideration weld toe failures. The accuracy of the proposed method has been verified through a series of experiments on ASTM standard welded samples and a welded sample of a bus window pillar. This research is the first in experimentally validating a weld model based on the effective notch stress method through parameter tuning.

1.2 Objectives

The main objective of this study is to introduce the use of the effective notch stress approach in welded joint modeling. The effective notch stress method is a relatively new method that allows the weld toe and root failure to be calculated. The applicability and reliability of the effective notch stress approach with the use of the FEM will be summarized and discussed. In order to obtain a better understanding of the methods in terms of implementation and limitations, both simple and complex welded structures are studied. Both types of specimens are fillet welded and full penetration welded joints. They will be both analyzed by using the effective notch stress approach, and validated through a comparison with the experimental results. Experimental validation will mean the right balance between FEA and the experimental study for more efficient modeling. The objectives of this research are therefore:

- to develop a weld model based on stress analysis to predict the behavior of stress distribution in welded joints by using the effective notch stress approach,
- to examine the suitability of the effective notch stress approach in terms of application to welded joints.
- to validate the weld model with an FEA (tuning the parameters) and experimental study, and

1.3 Limitations

Fillet welds have high stress concentration factors in the weld toe, and hence are prone to failure. Only the failure at the weld toe for finite element modeling is taken into consideration in this thesis. Other areas prone to failure are not considered.

The complexity of welded joints of window pillars requires geometric simplification for modeling, but this could lead to deviation in calculations.

For the FEA and experimental study, the stresses are below the yield strength of the material, thus a linear stress analysis is carried out.

The number of elements of the window pillar in this study are limited by the software license and computer memory (RAM) which mean coarseness of the mesh in areas that are not of interest. The application of a fictitious radius less than 0.5 mm for the window pillar is also limited for the same reason.

In this research, only as-welded joints are used. Post-weld treated joints and joints tested in temperatures other than the ambient room temperature are not included. Only specimens made of stainless steel (SS) are tested.

1.4 Organization of the Thesis

The remaining parts of this thesis are outlined as follows.

In Chapter 2, a literature review will be provided on weld joint modeling. A short summary of four commonly used modeling methods on welding is presented. The effective notch stress approach is applied for the modeling in this research work. The details on the effective notch stress approach are presented in Sections 2.1.3 and 2.1.4.

In Chapter 3, geometry modeling, the method for meshing, boundary condition for both the ASTM and the bus window pillar specimens and the testing procedure of only ASTM specimens are discussed. Note that, the experimental procedure of the bus window pillar is not included in this thesis due to the confidential agreement.

In Chapter 4, the results and discussions are presented. Details of the FEA of both the ASTM and bus window pillar specimens are thoroughly discussed in this chapter. The experimental results and the validation procedure for ASTM specimens are also presented. Note that, the experimental results and the validation procedure of the bus window pillar is not included in this thesis due to the confidential agreement.

In Chapter 5, a summary of the main findings and outcomes of this research are provided and recommendations are given for future research which would provide more validation of the weld model.

Chapter 2 Literature Review

2.1 Approaches for Modeling of Welded Joints

There are various approaches used to model and analyze the welded structures with the use of the FEM. Generally, the approaches used for modeling welded structures are based on stresses, strains, or stress intensity factors. There are four common modeling techniques used for the modeling of the welded structures of vehicles, ships, bridges, offshores, etc. They are: the nominal stress, hot spot stress, effective stress, and linear elastic fracture mechanics (LEFM) approaches. These approaches are mainly categorized as global and local approaches. Global approaches are the simplest and most common approach, and an example is the nominal stress approach. Local approaches are based on local failures, and highly sensitive to finite element modeling in high strain gradient areas, i.e. stress singularities. The hot spot stress, effective notch stress and crack propagation approaches which use linear elastic fracture mechanics are local approaches [3]–[7]. The stress parameters used for weld joint modeling are presented in Figure 2-1-1.

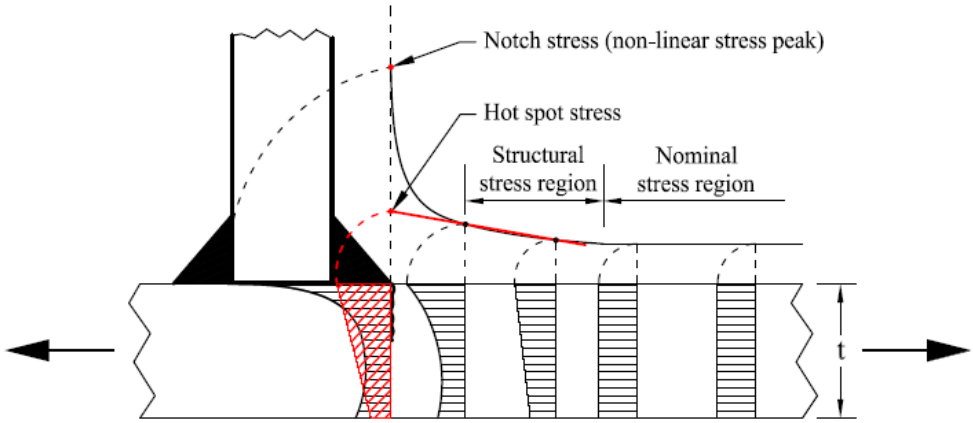

Figure 2- 1- 1 Stress distribution through plate thickness and along the surface close to the weld [4].

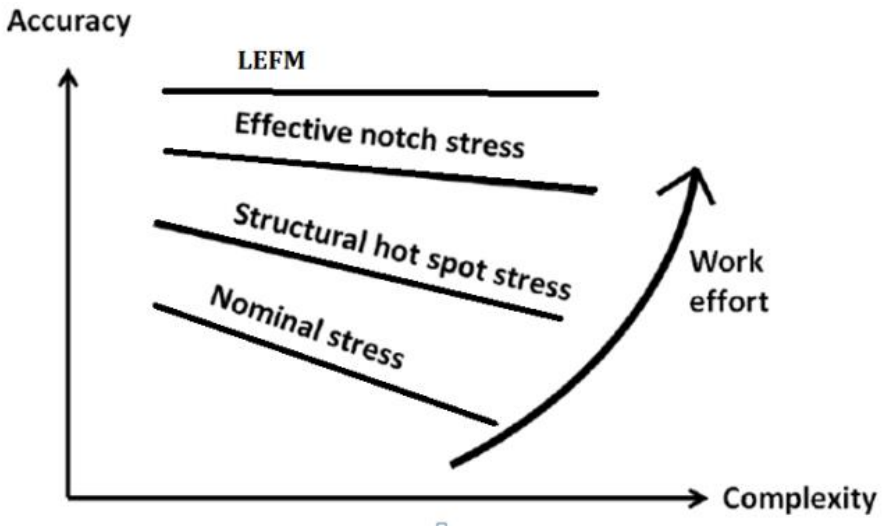

Figure 2- 1- 2 Work effort and accuracy comparison of the different approaches [5].

The goal of this chapter is to provide a review of the most frequently used modeling techniques of welded structures for stress analysis. I have used the effective notch stress approach for the modeling in this research. Therefore, the effective notch stress approach will be discussed more extensively.

2.1.1 Nominal stress approach

The nominal stress approach is the most common and the simplest applied procedure for the modeling of welded structure with the use of FEMs. The nominal stress is calculated as the average stress in the studied cross section of a welded joint in considering the linear elastic behavior. During stress calculations, the local stress raising effects of the welds on the attached plates are disregarded and only the macro-geometric effects are considered. This approach is limited to the analysis of multi-axial loading and complex structures.

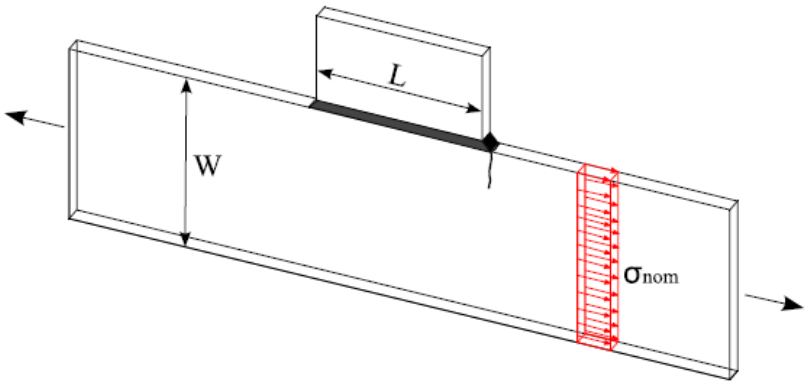

Figure 2- 1- 3 Nominal stress definition for plate edge joint [6].

The design codes and guidelines available for the nominal stress method are specifically for specific load configurations and geometries. Therefore, care must be taken during modeling with the use of this approach. Geometrical modifications or irregularities due to welding must be considered [4]–[7], and it is upon this consideration that local stress approaches are developed.

2.1.2 Structural or hot spot stress approach

In the past decades, there has been increasing use of FEM, and FEM has provided local concepts for weld joint modeling. The hot spot stress approach is the first developed local stress approach for weld joint modeling, and also called the geometric stress approach. The hot spot stress approach is used to calculate stress in weld joint modeling where the nominal stress cannot be used due to loading and/or geometric complexity. This approach is very popular for modeling pressure vessels and tubular welded joints.

The hot spot stress approach considers the effects of geometrical modifications and irregularities. The principal behind the hot spot stress approach is calculating the stress at critical points, which are also called hot-spot points. This approach considers the weld toes as the crack initiation points. The hot spot stress is the average of the membrane and the bending stresses at the weld toe for shell or plate structures which considers linear elastic behavior (Fig. 2-1-5). The hot spot stress can be calculated by using the inner linearization of the stress or surface stress extrapolation [4]–[7]. This approach solves the problem of calculating stress at the point of stress singularities (sharp points). Fricke and Petershagen [8] and then Radaj [9] used this approach on several complex welded structures. Details and recommendations for determining hot-spot stresses are given by Niemi [10].

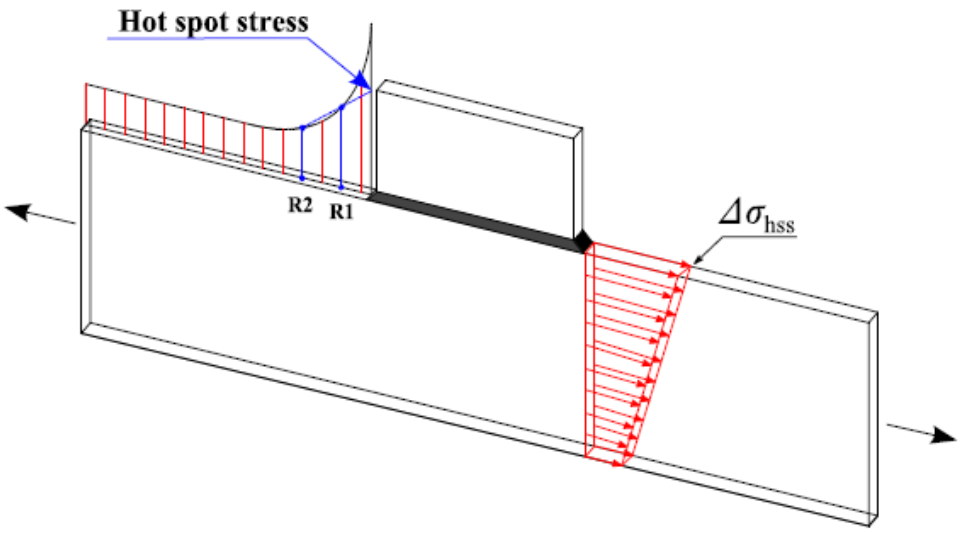

Figure 2- 1- 4 Hot spot stress definition at the weld toe in plate edge joint [4].

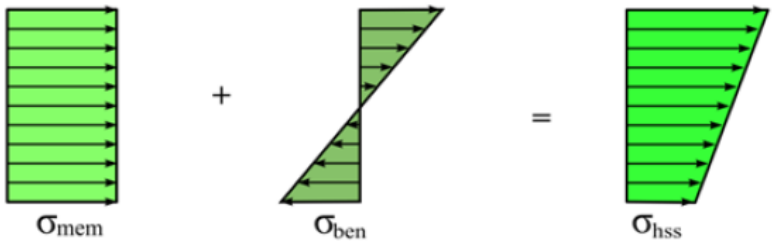

Figure 2- 1- 5 Stress distribution in front of weld toe according to the hot-spot stress [5].

Fine meshing is very important for finite element modeling with the use of the hot spot stress approach for calculating stress in critical areas. This approach considers the membrane and the bending stresses from the thickness of the welded plates (see figure 2-1-4 and 2-1-5). The non-linear peak stress across the thickness from the weld itself is not considered. This approach is therefore limited to only weld toes and cannot be used to calculate the stress at critical locations, such as weld roots, which cannot be analyzed by stress linearization or surface stress extrapolation. In these cases, it is more useful to apply the effective notch stress approach [4]–[7], [9].

2.1.3 Effective notch stress approach

Welded structures have weld start and end points which are the most failure critical locations. The weld toe is generally a critical area in welded structures, but for some structures, the weld root can be more problematic due to high stress concentration. Both may lead to the failure of a structure. Without taking into consideration previous weld defects, cracks mainly initiate from the weld toe or weld root. For the weld toe, crack propagates through the base material and for the weld root, crack propagates through the weld throat [4], [5], [11]–[13]. The most important geometrical characteristics of weld are the notch radius of the weld toe and weld root, and the

depth of penetration. The local approaches (based on notch stresses) are established based on these parameters of the weld geometry. On the other hand, the global approaches are based on nominal or geometric (structural) stresses, where the effects of these individual features of a construction are not considered [13], [14].

The modeling concept of the effective notch stress is gaining more and more importance in industrial applications among all the local concepts. The primary idea of this concept is the modelling of the weld toe or the weld root with a reference notch radius to determine the local von Mises stress or the principal stress assuming linear elastic behavior [4], [5]. In the following, the theoretical rationale of the reference radius methods will be explained.

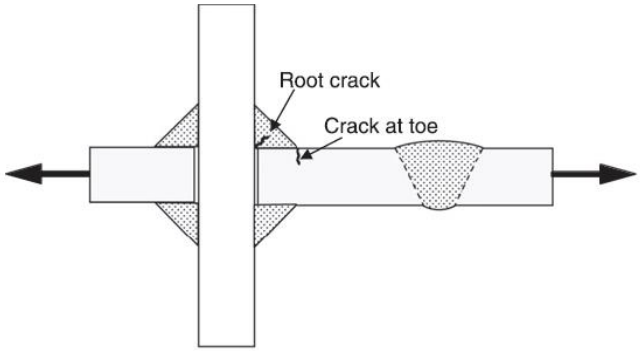

Figure 2- 1- 6 Cruciform welded joint loaded in tension [8].

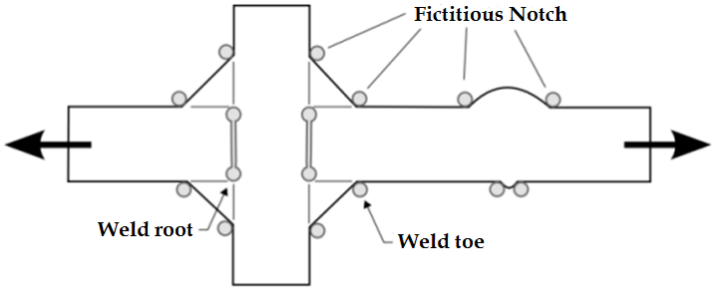

Figure 2- 1- 7 Rounding of the weld toe and weld root in the effective notch stress method [8].

The effective notch stress approach directly evaluates maximum stresses at a notch, where crack initiation is anticipated, i.e. either at the weld toe or the weld root. The geometry of the notch cannot be directly modeled by using FEA because of the irregularity of the weld. This can be resolved by the introduction of a fictitious effective notch as shown in Figs. 2-1-6 and 2-1-7. This method was developed by Radaj based on the micro-support concept of Neuber [9], [14], [15]. This is a linear elastic approach for modeling the weld toe or root with a reference radius. This specific reference radius considers the irregularities in the weld, as well as non-linear behavior, and is called the effective notch radius, ρ_f. The magnitude of the effective notch radius is derived from the micro-structural support hypothesis by Neuber.

The basis of the hypothesis put forth by Neuber is that the maximum notch stress is not the main conclusive factor for crack initiation in a notch. Instead, crack initiation is developed for some lower stresses. These stresses can be calculated by averaging the maximum stress over a certain depth of the material (material-characteristics small length, area or volume) which alternatively can obtained by enlarging of the fictitious notch radius (shown on Fig. 2-1-8) [8], [12]– [20]. In other words, theoretically the static or fatigue strength cannot be characterized by the maximum notch stress for sharp or pointed notches. The notch stress needs to be averaged over a material-characteristics small length normal to the notch edge. This material-characteristics small length is called "structural support length". The structural support length results a specific "elementary" volume for a material. The elementary material volume (microsupport length ρ^*) is used to average the maximum notch stress at the notch toe or root (with radius ρ). An enlarged fictitious notch radius is used to express the average stress of the corresponding notch. This enlarged fictitious notch radius is expressed in term of the material parameter ρ^* and the microsupport

factor s. The effect of multiaxiality and the strength criterion dictates the microsupport factor s and the microstructural material conditions controls the magnitude of the length ρ*.

Neuber have given a relationship $\rho^* = (2/\pi)\ (K_{Ic}/\ \sigma_{mc})^2$ for static loading condition, where K_{Ic} is the fracture toughness and σ_{mc} is the local fracture stress [18]–[20]. He has given another relationship for brittle fracture. The relationship is $\rho^* = (1/2\pi)\ (K_{Ic}/\ \sigma_Y)^2$, where σ_Y is yield strength (approximately close to the ultimate strength). This both relationships are later confirmed by the "critical distance approach" [18]–[21].

When ρ= 0 mm, s= 2.5, and ρ*= 0.4 mm in low-strength steels, this is considered to be the worst case scenario. The IIW recommend that it is valid and applicable to the welded joints made of structural steels and aluminium alloys.

In this study, Mode I loading is considered so as to pinpoint the main points of the approach put forth by Neuber. In the worst case scenario, with a very small notch radius or one that tends to zero, the theoretical stress concentration factor K_t significantly increases and the theoretical peak value of the notch stress cannot be applied to the brittle or fatigue failure of a component. Consequently, the stress that has been averaged over a finite size material element is then considered to be the origins of local failure rather than the theoretical peak stress in the case of sharp pointed or rounded notches, which also include cracks and corner notches.

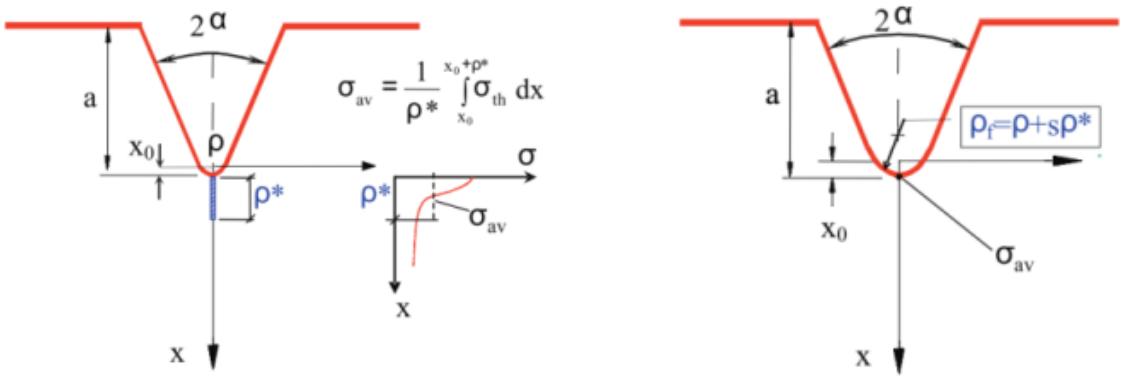

(a) Actual notch with stress averaging over ρ*

(b) Substitute notch with fictitious notch radius resulting in σ_{av}

Figure 2- 1- 8 Neuber's micro-support concept [13].

At the notch tip, the microstructural support length ρ* which is material-dependent, affects the microstructural material element. The experimental results from a study carried out by Berto [22] show that ρ* ≈ 0.1 mm for low-strength steels and aluminium alloys with fatigue problems. The averaging of the stress is carried out over ρ*, which addresses the notch problem and integrates the theoretical notch stresses σ_{th} over ρ*:

$$\bar{\sigma} = \int_{x_0}^{x_0+\rho^*} \sigma_{th}\, dx \qquad (1)$$

The equation that follows can also be used in situations where the equivalent stress is presented by a square root expression:

$$\bar{\sigma}^2 = \int_{x_0}^{x_0+\rho^*} \sigma^2{}_{th}\, dx \qquad (2)$$

For simplification purposes, Neuber introduced the concept of fictitious notch rounding, see Figure 2-1-8 (a). The use of a notch that has a fictitiously enlarged notch radius ρ_f, will result in the average notch stress, $\bar{\sigma}$, see Figure 2-1-8(b):

$$\rho_f = \rho + s.\rho^* \quad (3)$$

where ρ is the actual notch radius, s the support factor (which is dependent on three loading modes: 1, 2, or 3, or transverse tension, in-plane or out of plane shear, respectively, or mixed mode loading and the strength criterion of the material), and ρ^* the micro-support length that is material-dependent. The notch opening angle is 2α, and is affected by different values of the support factor (Fig. 2.1.8) [18]–[21].

Neuber determined the fictitious notch radius ρ_f from the support factor s through the following steps [18]–[22]:

(i) assumed the bisector of the sharp rounded V-notch as a crack path (without microstructural support) (see figure 2-1-8).

(ii) derived an expression of the equivalent stress σ (or τ) for the bisector;

(iii) derived another expression for the peak stress σ (or τ) to average over the microstructural support length;

(iv) equated the two expressions of σ (or τ) (from (i) and (ii)) for $\rho^* = 0$ and used numerical procedures to derive the expression of fictitious/effective notch radius ρ_f which is dependent on ρ, ρ^*, and 2α; and

(v) also derived expressions for the support factor $s = (\rho_f - \rho)/\rho^*$ which is also dependent on ρ, ρ^*, and 2α.

The notch stress in welded joints originates from both the component geometry and local stress raisers, i.e. welds, which comprise the total local stress. Therefore, the effective notch stress consists of the membrane, bending and non-linear peak stresses (Figure 2-1-10).

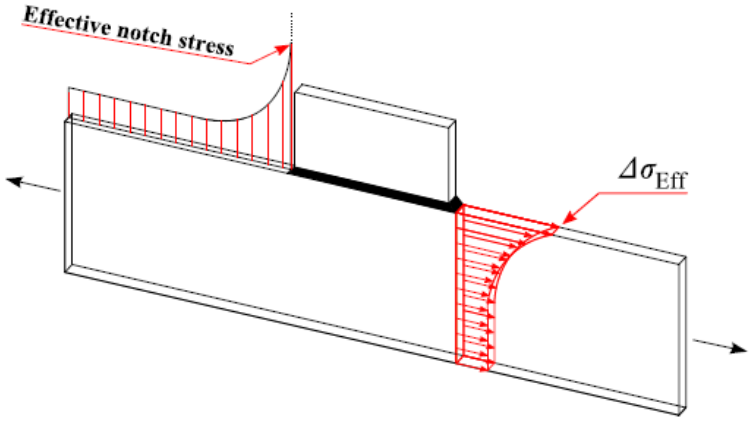

Figure 2- 1- 9 Effective notch stress definition at the weld toe in plate edge joint [4].

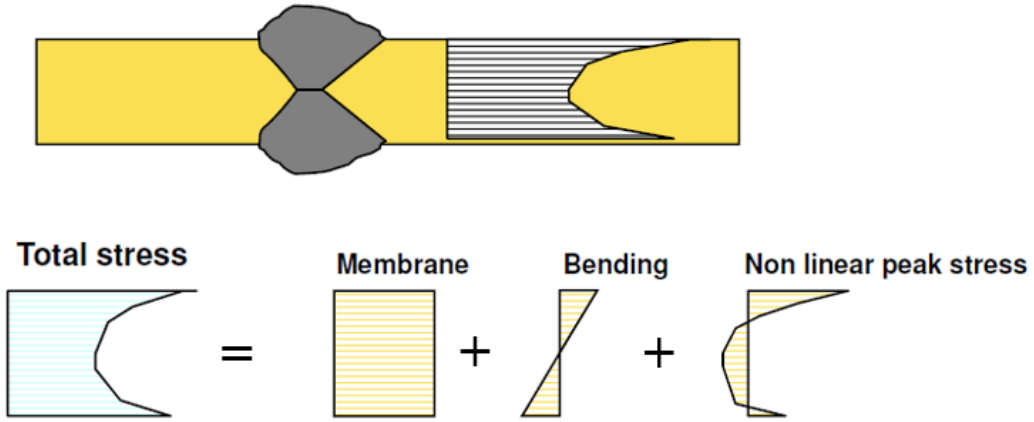

Figure 2- 1- 10 Stress distribution in front of weld toe according to the effective notch stress [5].

An effective notch radius of 1 mm is used in worst case scenarios in which there is a very sharp notch without a radius (ρ=0). The ρ* and s are approximately 0.4 mm and 2.5 mm respectively

for steel welded structures. The effective notch radius is 0.05 mm for thin plates, which originates from the relationship between the notch stress and the stress-intensity factor (theory of crack blunting, put forth by Irvin) [9], [13], [14], [23].

Therefore, there are initially two values for the effective notch radius ρ_f that were put forth for use in structural steel; ρ_f=1 mm for thick plates (t >5 mm) and ρ_f=0.05 mm for thin plates (t ≤5 mm) [3], [4], [9], [14]–[16], [24], [25]. These two values have been successfully applied in steel and aluminum. However, there are other values found in the literature, such as 0.2 mm, 0.3 mm, 0.5 mm, etc. [23]. Therefore, the value of ρ_f has to be tuned to validate the FEM model with the experimental results for specific materials and structures.

Note that this method is limited to naturally formed welds, so that weld improvements are not considered here.

2.1.4 Recent studies on Effective Notch Stress approach

The basic concept of effective notch rounding is to simulate the average stress over a microstructural support length in the crack propagation direction of welded joints. FEA is commonly used to determine the stress concentration factors with fictitious notches applied as real notches within the finite boundaries of cross-sectional modeling. The real notches causes the weakening of the cross-sction and the fictitious notches try to capture the effect of the real notches [9], [14], [15].

Several research papers on this new concept of using the effective notch stresses of welded joints have been recently published.

The effective notch stress approach assumes that there are plane strain conditions at the notch. This method can determine the local stress without requiring a stress concentration factor (SCF).

Radaj used a notch radius of 1 mm in steel for weld toe modeling as a worst case scenario [9]. The applicability of this notch radius of 1 mm was later investigated in aluminum alloy by Sonsino *et al.* [13].

Pang *et al.* [26] used a simplified 2D finite element model with the effective notch stress approach on tubular booms of draglines under different loading cases. They found that the critical location is either at the weld toe or root. Morgenstern *et al.* [27] investigated different types of MIG butt-welded joints made of the aluminium alloy under pulsating axial and fully reversed loading. They applied a fictitious notch radius of 1 mm on aluminum plates with a thickness of 5 mm which was successful.

Park *et al.* [25] applied the effective notch stress approach on large-sized specimens, that is, diaphragm, cruciform, and out-of-plane gusset joints. They used a notch radius of 1 mm for the weld toes and weld roots. They then investigated the effects of the fixed effective notch radius with respect to the weld size, plate thickness and width, and full penetration and fillet welding. They concluded that the effective notch stress approach can determine whether cracks will initiate at the weld toe or the weld root.

Malikoutsakis *et al.* [28] applied the effective notch stress approach on rear axles that are thick-walled and compared numerical stress-strain results with experimental results under monotonic and cyclic loading to verify the accuracy of the modelling technique used. He obtained satisfactory results for complicated stress areas. Maljaars *et al.* [29] compared nominal, structural and fictitious notch stresses for simple and complex welded joints with filled welds. He found that three stress differences are significant for complex cases and the fictitious notch stress

approach showed good agreement with the experimental results. He also recommended the creating of finer meshes in critical areas.

Kaffenberger *et al.* applied an effective notch radius of 0.2 mm and validated this radius value for thin welded structures. They considered the radius from real scanned geometries, and the effect of the radius and size effect [17]. Malikoutsakis and Savaidis [12] used the effective notch stress method in the 3D modeling and meshing of the weld toe and root based on IIW recommendations for the rear axles of a motor truck. They used an effective notch radius of 0.2 mm for thin plates. They found good agreement between the FEM with measured stresses from the strain gages in the failure regions. They suggested other materials aside from steel and situations other than shear stress for further experimental verification.

Sonsino *et al.* used the effective notch stress approach with a fictitious notch radius of 0.05 mm for thin walled welded joints and 1 mm for thick walled welded joints on four different sectors: the sandwich panels for ship decks, offshore K-nodes, an automobile door, and a trailing link. The FEM and experimental results were verified to check the consistency of the effective notch stress method [13].

Hyoung *et al.* [30] applied the effective notch stress approach on rib-to-deck joints and found a good correlation between the FEM results with the observed experimental results.

Schijve [23] proposed a specific ratio for two parameters instead of settling for some specific values based on the thickness of the welded plate for modeling purposes. He specified the ratio as q/h where q is the radius and h is the dimension of the weld. He recommended q/h=0.1 but this should be further investigated.

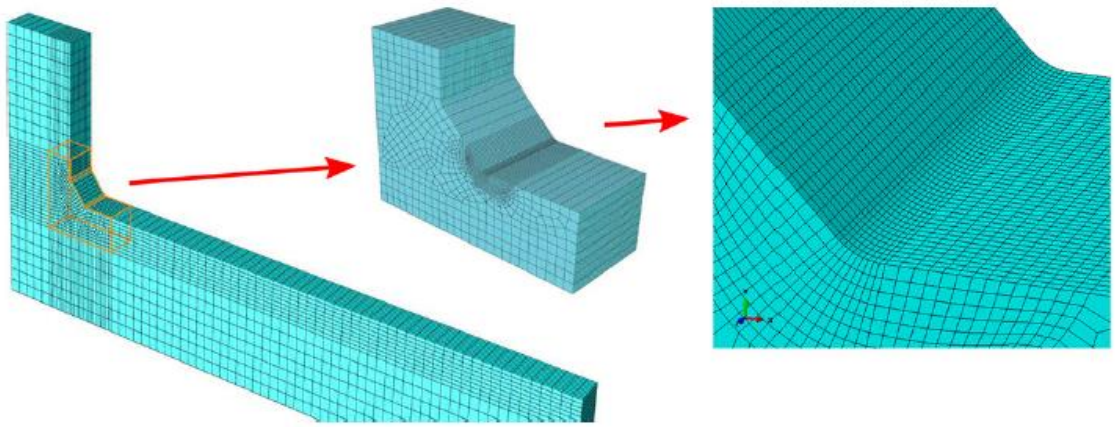

Figure 2- 1- 11 Global model and submodel for investigated plate edge joints [4].

Morgenstern *et al.* [27] investigated a large number of welded T- and Y-joints by using the effective notch stress approach. The plate thickness of these joints varied between 8 and 40 mm. They used an effective notch radius of 1 mm for finite element modeling. The effective notch stress approach took into consideration the effects of the residual stress, and biaxial and multi-axial loading [9], [13], [21], [31]. They proposed a sub-modeling technique for modelling and computation with regard to the mesh density in the effective notch stress method. The sub-modelling technique is very useful for capturing the maximum stress around the critical areas by allowing a fine mesh, see Figure 2-1-11 [4][27].

Round robin investigations have been recently performed on three structures: a fillet welded cruciform joint, complex rectangular hollow T-joint, and fillet welded rectangular hollow joint, to make a procedures for modelling the structure and analyzing the results. For numerical analysis, the element size should be at least 0.25 mm on the circumference of the rounded notch for an effective notch radius of 1 mm. A good agreement between the numerical results and the experimental results were found [16], [24].

The stress concentration areas are the most critical regions of the model. In order to determine the maximum stress appropriately, it is necessary to have a sufficient element density at the area of stress concentration. 3D solid elements are able to model and mesh with sufficient accuracy [4], [6], [11], [32].

During finite element modeling, extremely or infinitely high stresses may occur at a sharp notch due to a high stress concentration factor [14]. The effective notch radius is very small compared to the whole structure. The mesh density must be therefore finer to capture the notch for a better analysis. The DNV (2011) suggested the use of a minimum of 4 elements along a quarter of the notch circle circumference if quadratic elements are used. For an effective notch with a radius of 1 mm, this would correspond to a mesh size of approximately 0.4 mm at the notch surface.

2.1.5 Fracture Mechanics Approach

Weld joint modeling based on fracture mechanics addresses the relationship between geometric defects, material properties and applied stress. Failure occurs due to the critical combination of these three parameters. The philosophy of fracture mechanics is that the stress state at a crack tip or crack-like discontinuities in a structural member can be determined by using a single parameter, that is, the stress intensity factor (SIF), which depends on the three aforementioned parameters. The crack propagation approach has been thoroughly reviewed by Smith [33] and more recently also by Paris [34].They reviewed their insights of the progress of this approach during the last 40 years [35]–[38].

The stress state in members with discontinuities, such as holes and notches, can be determined by applying the effective notch stress method. However, to determine the stress state at a crack tip in which the radius of the crack tip approaches zero, thus resulting in infinite stress, the use of

fracture mechanics becomes necessary, i.e. stress analysis for structural members with cracks. This approach is well suited for through-thickness crack failure when the crack propagation period is higher than the crack initiation period.

The modeling of welded joints using linear-elastic fracture mechanics approach is different from other concepts. This approach assumes that there is always an existing crack due to results of welding. The crack size varies from 0.05mm to 1mm. The cracks mainly come from inclusions, cold laps, undercuts. and lack of fusion [34]–[38]. The concept of LEFM is that the stress conditions at a crack tip are dependent on the stress that is applied onto a structural member and the configuration of the cracks, such as their size, shape, and orientation and assumes that the material conditions are linear elastic during crack growth. Therefore, the effect of plasticity is not considered in LEFM, despite that ductile materials often show some degree of plasticity [35], [36].

Chapter 3 Methodology

3.1 Introduction

In order to achieve the objectives of the research work in this thesis, two different types of welded specimens are separately investigated. Therefore, there are primarily two phases in the development of the weld model with the use of the effective notch stress approach. In the first phase, the ASTM specimens are modeled by using ANSYS and an experimental study is carried out with this sample. The finite element model of the ASTM specimens is tuned for the experimental validation by using the effective notch stress approach. In the second phase, the same procedure is applied onto an actual bus window pillar. The study on the two different types of welded samples provides an optimum effective notch radius for weld joint modeling. In this chapter, finite element modeling of the geometry including meshing, material assignment, boundary and load conditions, the experimental study and validation procedure are presented for each phase.

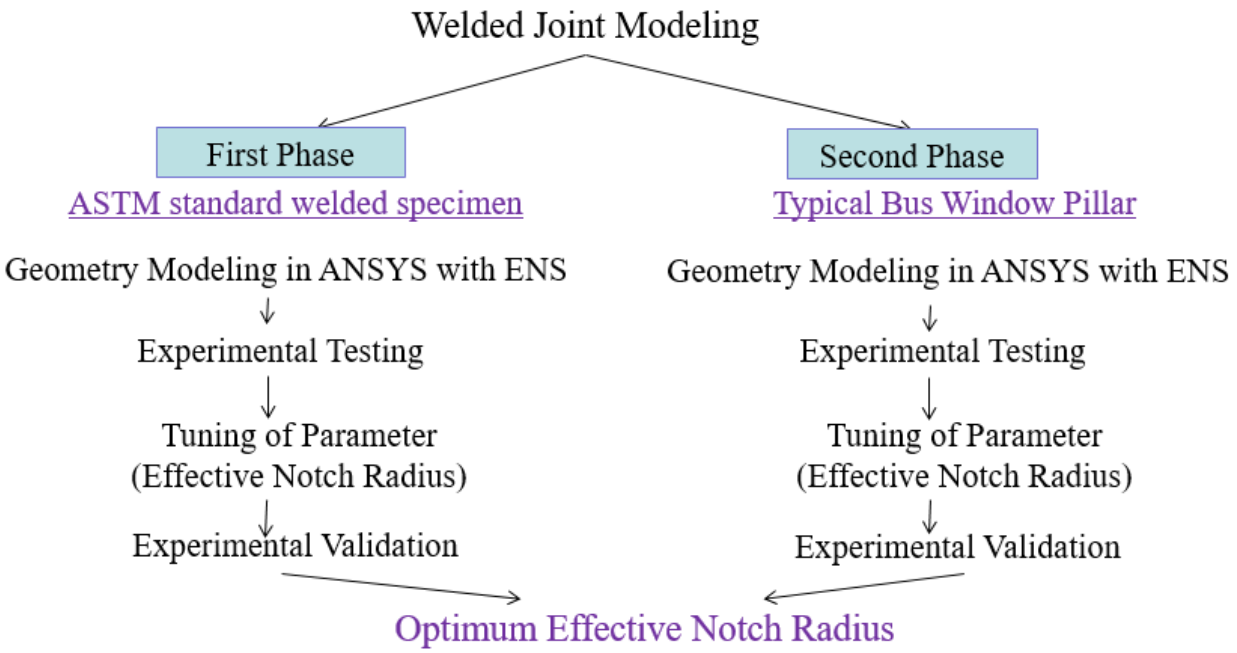

3.2 Finite Element Modeling

The practical use of finite element modeling is known as FEA which is best understood during the real problem solving [39]. FEA has been widely used by the automotive industry. It is a very popular tool for design engineers in the product development process. FEA allows design engineers to analyze their designs while the designs are still in the form of an adjustable computer aided design (CAD) model. This helps and gives flexibility to the design engineers to go back and forth to implement of the FEA analysis results in the whole design process and improve the model. It is important to understand the FEA basics, modeling techniques, the inherent errors and their effects on the quality of the results so as to render FEA as a successful design tool. FEA is also used as a computational tool for carrying out engineering problem analyses [39], [40].

A typical FEA involves:

(1) model preparation: development of the design of a product and preparation of the CAD model;

(2) mesh generation: division of the model domain into a collection of subdomains. The material and structural properties that characterize the way that a structure will react to loading conditions are found within these subdomains. The subdivision of a model domain has several advantages as follows:

   (a) a complex geometry is accurately represented,

   (b) material properties that are dissimilar can be incorporated,

   (c) local effects are captured,

   (d) the total solution can be represented with ease [39];

(3) application of boundary conditions to the model. Then each subdomain can be represented by a set of element equations; and

(4) a solution (post-processing), in which to carry out the final calculation, there is the recombination of all the subdomain elemental equations from (3) to form a global system of equations. The numerical technique is used to solve this global system of equations using the initial values of the original problem. The computational time depends on the number of subdomains [39], [40].

In this study, ANSYS Workbench (version 15) is used to carry out finite element modeling and analysis. The modeling procedure with the use of ANSYS Workbench will be explained in detail as follows.

3.2.1 Geometry Modeling

The first step of an FEA is the geometry modeling. The geometry of both types of welded joints was modeled with ANSYS. All of the dimensions of the actual specimens were kept constant, except at the weld toe. The effective notch radius of the weld toe was varied for both samples to validate the model with the experimental results.

3.2.1.1 ASTM Specimen

In accordance with the effective notch stress approach, the contour of the weld toe was replaced by using a circular notch, $\rho_{f,}$ in the finite element model. Different values of the effective notch radius, such as 0.1, 0.2, 0.3, 0.4, 0.5, and 1.0 mm, were used in the weld joint modeling. Figure 3-2-1 shows the position of the effective notch in the finite element modeling of the weld of an ASTM specimen [41].

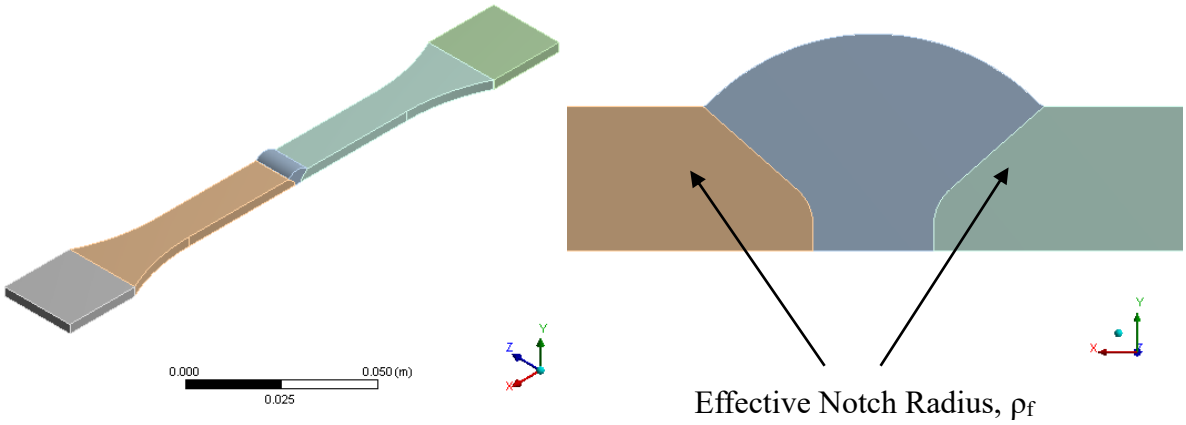

Figure 3- 2- 1 ASTM specimen model in ANSYS workbench [41].

This model consists of mainly two zones: area of the base metal and welded zones. The two zones are contact bonded together. In terms of the properties of contact bonding, there is no penetration, separation and sliding between the faces or edges [42].

3.2.1.2 Bus Window Pillar

The pillar geometry of the bus window is very complex and different compared to that of the ASTM standard specimens. It has fillet welds in a total of four areas: two on the front side and two on the back side. According to the effective notch stress approach, the contour of the weld toe can be replaced by using a circular notch, ρ_f. Different values of the effective notch radius, such as 0.5, 0.75, and 1.0 mm, have been used for weld joint modeling. Figure 3-2-2 shows the position of the effective notch in the finite element modeling of the weld.

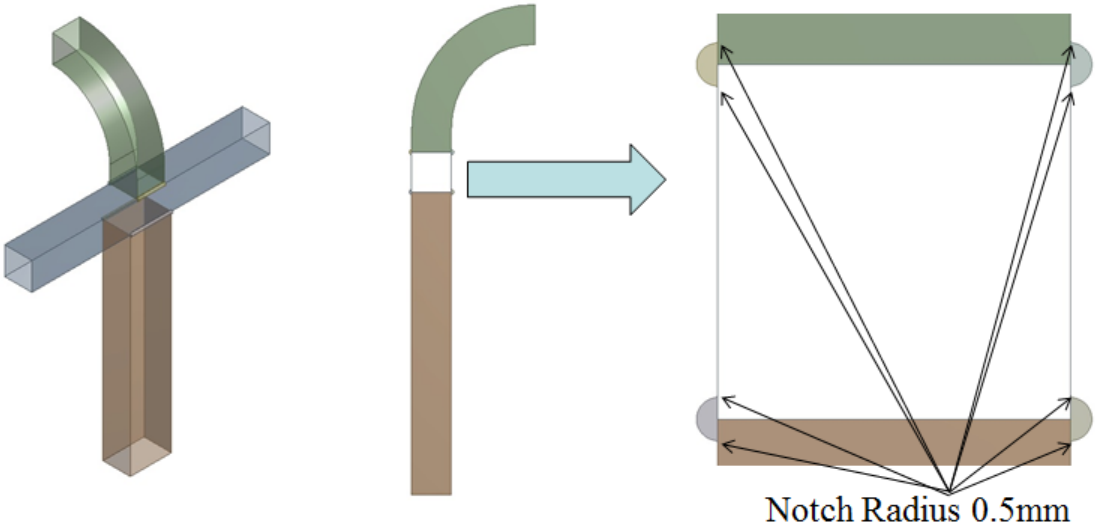

Figure 3- 2- 2 Bus Window Pillar model in ANSYS workbench.

There are three different types of contacts in the window pillar model: bonded, frictional and multi-point constraint (MPC).

The properties of these three different types of contacts are as follows.

Bonded Contact: There is no penetration, separation and sliding between the faces or edges [42].

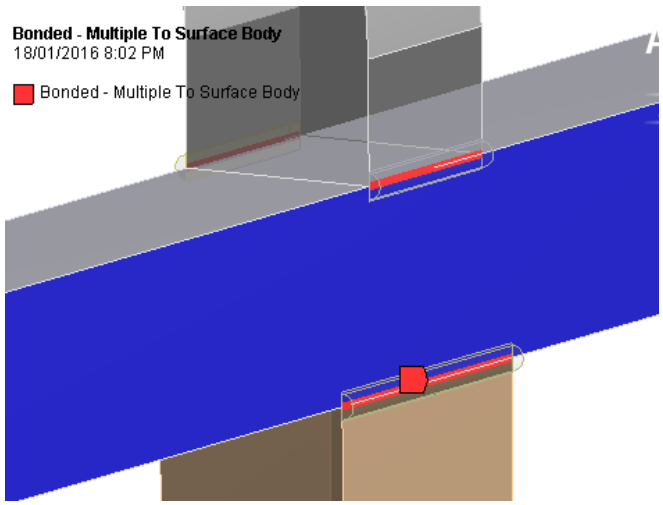

Figure 3- 2- 3 Bonded Contact in the Bus Window Pillar model

Frictional Contact: Sliding with resistance proportional to the coefficient of friction that is defined by the user, with the ability to separate without resistance [42]. The frictional coefficient 0.7 (SS to SS) is used in the modeling in this study.

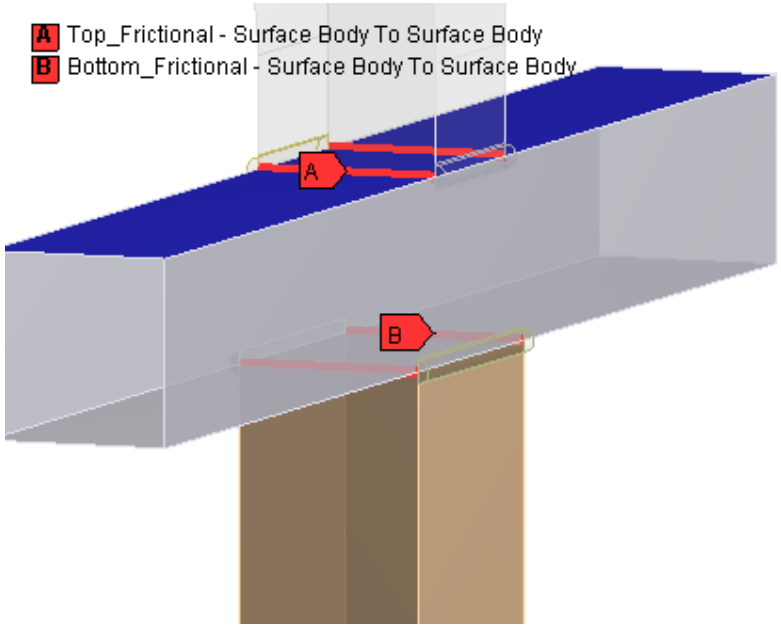

Figure 3- 2- 4 Frictional Contact in the Bus Window Pillar model

MPC Contact:

- takes into consideration the connection between a shell edge and a solid face,
- internally adds constraint equations to “tie” the displacements between surfaces that come into contact,
- transfers the effects from the shell to solid elements, and
- a direct and efficient means of relating the surfaces of contact regions which are bonded [42].

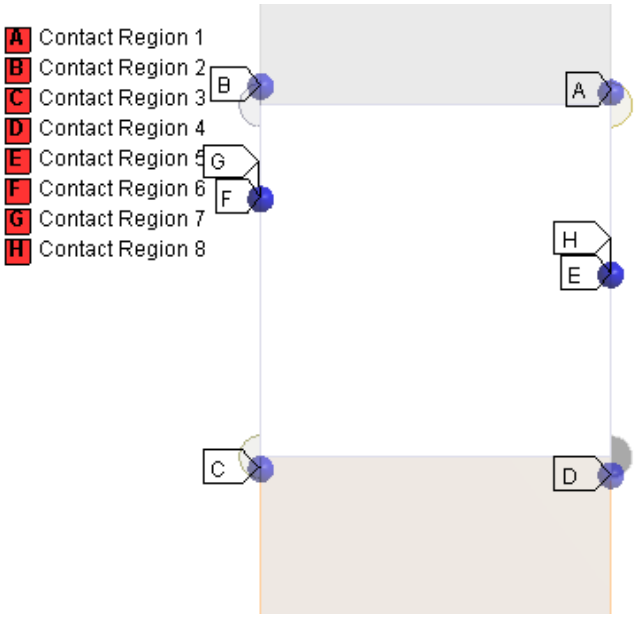

Figure 3- 2- 5 MPC Contact in the Bus Window Pillar model

3.2.2 Meshing

The next step of finite element modeling is the meshing of the geometry, which is the most important step for an FEA. The whole geometry model was divided into subdomains. Each subdomain is called an element. The sensitivity of the output results depends on the way that the mesh is generated and the quality of the elements. The element size was varied throughout the modeling. It is essential to have a fine mesh density mainly in the areas of high stress gradients and coarser mesh density in areas of low stress gradients or where the magnitude of the stresses is not of interest. However, the transition from a coarse mesh to a fine mesh should be gradual. Different meshing techniques were used to obtain a very fine mesh that surrounds the notch and coarser mesh for less significant areas.

3.2.2.1 ASTM Specimen

The FEM of the ASTM specimens as shown in Fig. 3-2-6 is modeled by using only SOLID45 elements with ANSYS. The sphere of influence and pinch control are used to create a fine mesh

density in the critical areas. The former can be used to better control the mesh sizing in the critical areas. Therefore, an element size of 0.1 mm in the region that is contained within the sphere can be created. An element size of 1 mm was used for the whole model, but also used for the weld and near weld zones which are the critical areas. Figure 3-2-7 shows the effect of the sphere of influence on meshing. Pinch control is used to merge the mesh nodes in close proximity after meshing by using a given meshing tolerance value which removes the bad quality elements from the model, thus resulting in more refined meshing [41]. The total number of elements is 100132 and the total number of nodes is 364763 in the FEM of the ASTM specimens.

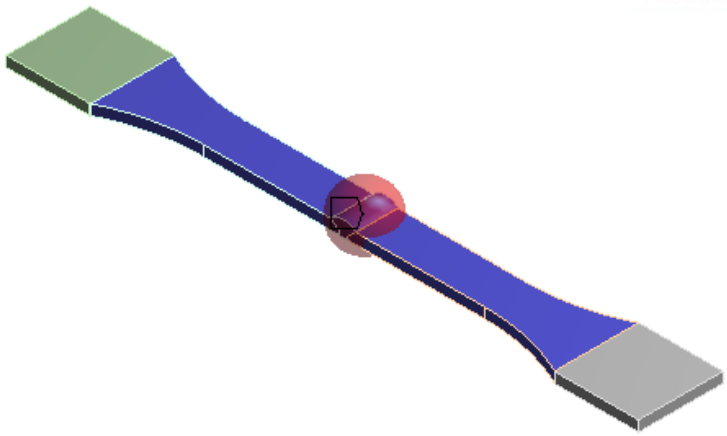

Figure 3- 2- 6 Effect of spherical influence in the FEM Model [41].

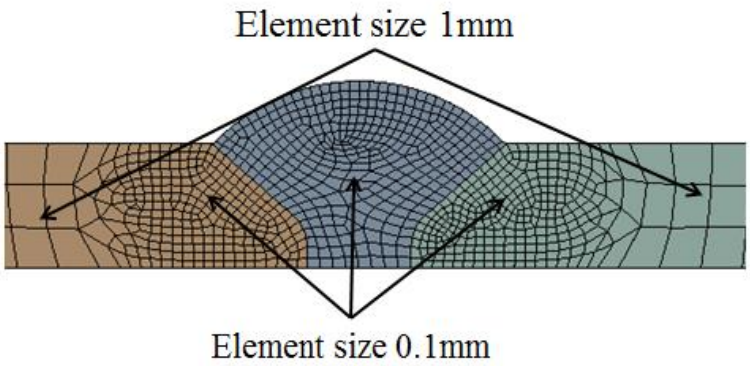

Figure 3- 2- 7 Meshing of ASTM FEM model [41].

3.2.2.2 Bus Window Pillar

The bus window pillar was modeled by using a combination of SOLID45 and SHELL181 elements in ANSYS. Initially, the whole bus window pillar was modeled by using only solid elements. Due to software license limitations, it was not possible to solve the model because it contained a very large number of solid elements. Later, the body trusses were modeled by using shell elements and the welded and adjacent weld zones by using solid elements to reduce the number of elements.

The bus window pillar has a very complicated geometry in comparison to the ASTM specimens. It was therefore very challenging to create fine meshes in the modeling of the bus window pillar and not possible to use the sphere of influence because this created a very large number of elements in the defined spherical region and therefore the model could not be solved due to limitations imposed by the software license and the amount of computer RAM. Another challenge was to have at least 4 elements along a quarter of the notch circumference. According to Hobbacher and Fagnastøl, when at least 4 elements are used along a quarter of the circumference of a circular notch, stress is more concentrated between the nodes [6], [11]. It is easier to extract higher stresses at the nodes.

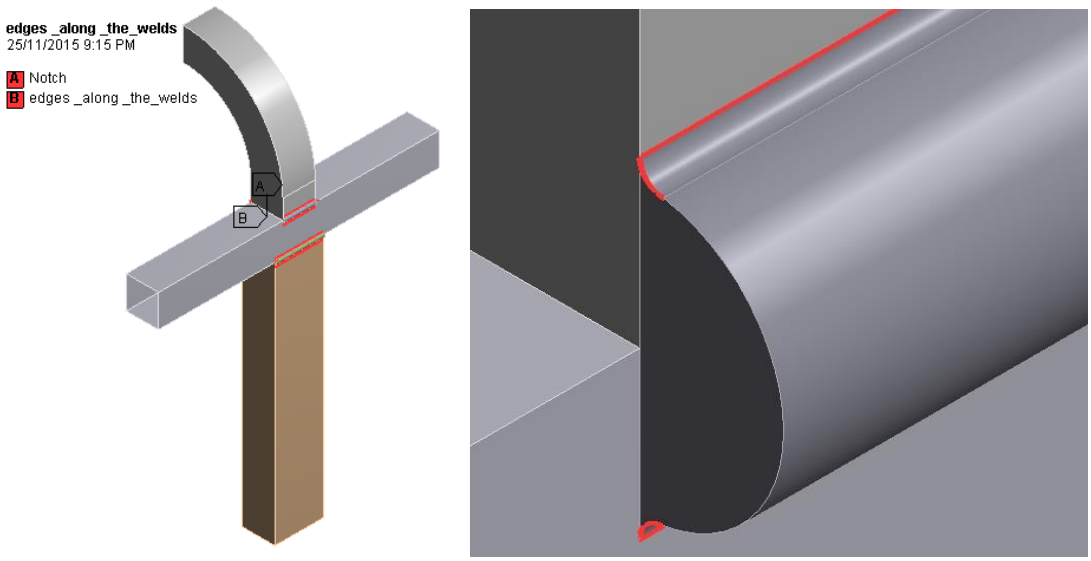

Figure 3- 2- 8 All notch circle circumferences and edges along the weld were selected by Name Selection in ANSYS workbench

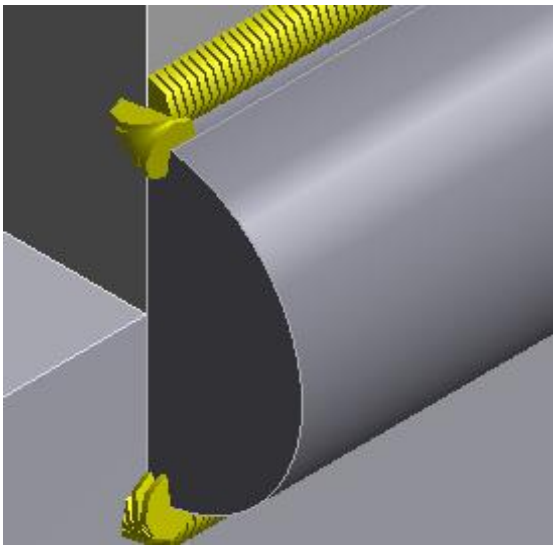

Figure 3- 2- 9 Elements created along the notch circle circumference and weld edges.

To overcome these two challenges, the circumference of the circular notches was first selected by using the Named Selection feature in ANSYS (Figure 3-2-8). The length of each of the notch

circumference is 0.7854 mm. To obtain a fine mesh, 5 elements were created along a quarter of the notch circumference. Each element size is 0.15708 mm. To obtain a smooth transition and finer mesh around the notches, all of the edges near the notches were selected by using the Named Selection feature. On each edge, the element size was also maintained at 0.15708 mm by using edge sizing to create a fine mesh near the notch (Figure 3-2-9). Figure 3-2-10 shows the meshing of the bus window pillar model. Figure 3-2-11 shows a smooth transition from fine to coarse elements in the adjacent weld zone, and the fine mesh elements around the notch. The total number of elements is 212028 and total number of nodes is 766026 in the FEM model of the bus window pillar. The ANSYS post-processor required a substantial amount of time to solve this model during each attempt.

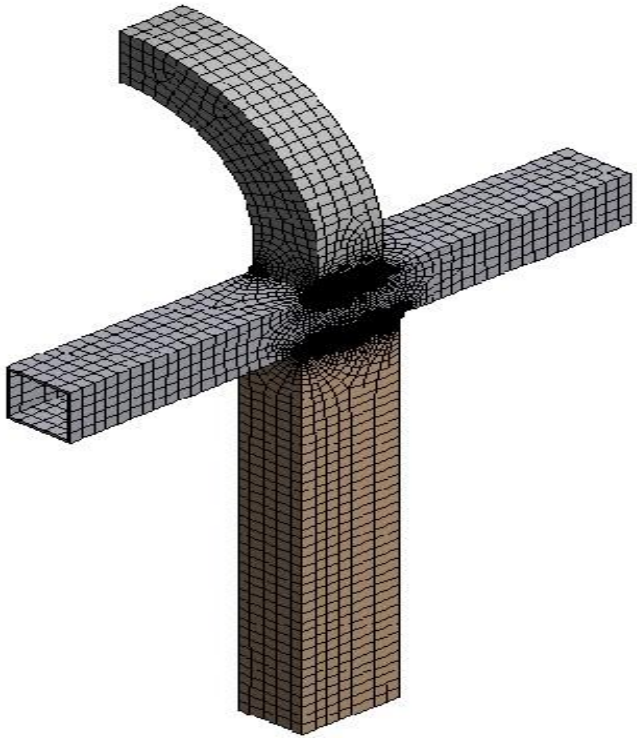

Figure 3- 2- 10 Meshing of Window Pillar FEM model

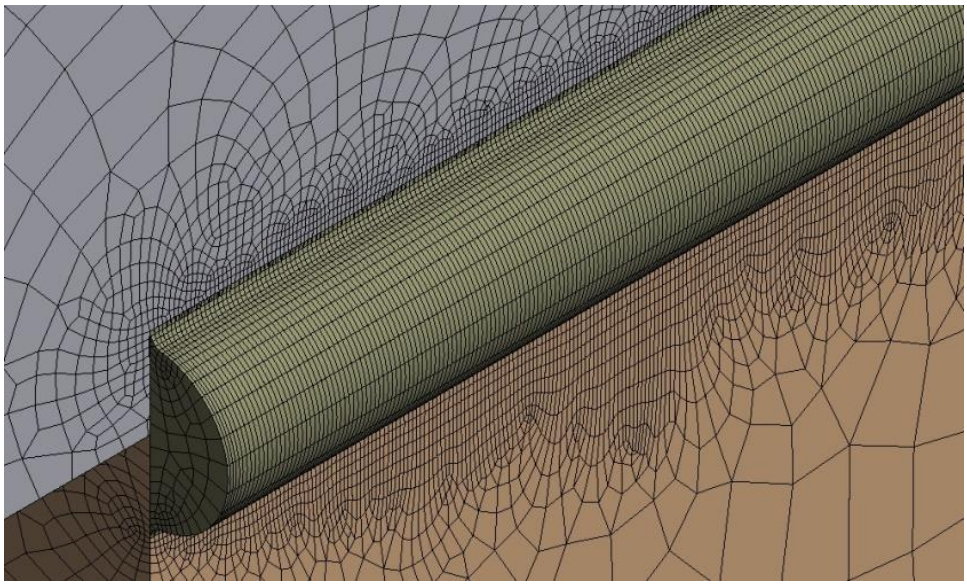

Figure 3- 2- 11 Smooth transition and fine mesh elements around the weld toe.

3.2.3 Assumptions, Material Properties and Boundary Condition

3.2.3.1 Assumptions

The following are the assumptions for this study:

- the behavior of the FEM model of the welded joint is linear elastic during the analysis, and
- there are no welding defects in the welded joints.

3.2.3.2 Material properties

The base material is SS 41003 and the filler material is SS AWS ER 308L for both types of welded samples. The material properties of the base and filler materials are given below.

Table 1 Material Properties of base material and filler material

Type	Material	Yield Strength, MPa	Ultimate Strength, MPa	Young's Modulus, GPa	Poisson's ratio
Base Material	SS 41003	346	513	210	0.3
Weld Material	SS AWS ER308L	390	580	210	0.3

3.2.3.3 Boundary Condition

The boundary condition in ANSYS was specifically chosen to simulate real applied boundaries during testing. A different boundary condition was set for the ASTM and bus window pillar models respectively.

3.2.3.3.1 ASTM Specimens

As shown in Fig. 3-2-12, one end is fixed for the ASTM specimens, and on the other end, the force is only in the X direction, and the displacement in the Y and Z axes is zero.

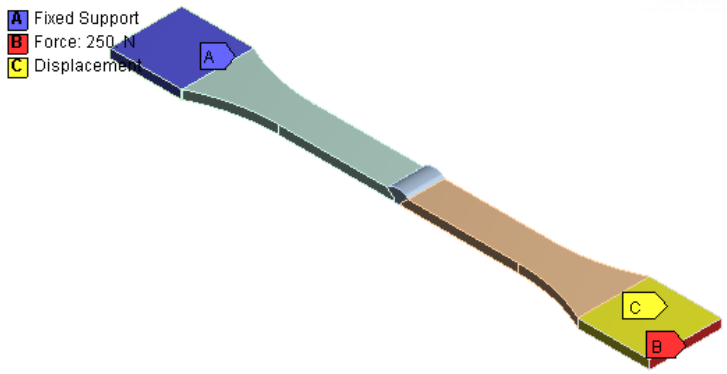

Figure 3- 2- 12 Boundary Condition of ASTM specimen in ANSYS workbench environment [41].

3.2.3.3.2 Bus Window Pillar

The boundary condition of the bus window pillar is shown in Fig. 3-2-13. The left, right and top ends are fixed when a bending load is applied from the left to the right on the bottom end. This boundary condition is recommended by the company of the bus window pillar, and was actually

extracted from the original FEM model of the bus structure when standard loading was applied. Then, it was simplified for real testing and also used for the FEA.

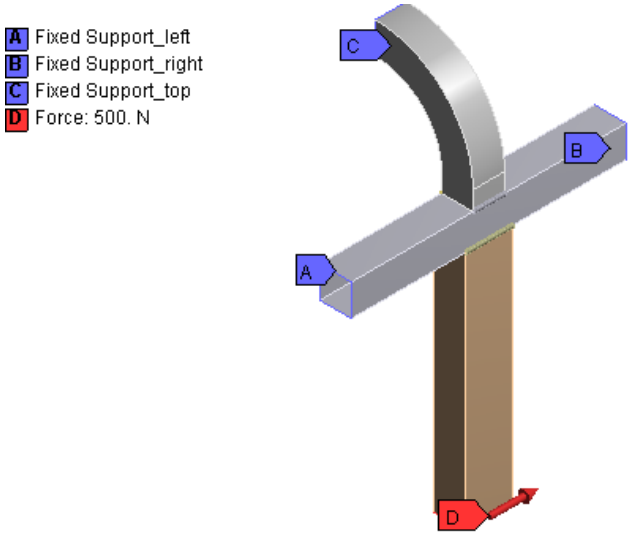

Figure 3- 2- 13 Boundary Condition of Window Pillar in ANSYS workbench environment.

3.2.4 Loading Cases

Loading cases were chosen to ensure that the analysis in this study is linear elastic. These loading cases are the same as the experimental loading points. The loading cases are different for the ASTM and bus window pillar models, as follows: ASTM model: 250 N, 500 N, 750 N, 1000 N, 1250 N, and 1500 N, and bus window pillar model: 500 N, 1000 N, 1500 N, 2000 N, and 2500 N.

3.2.5 Mesh Convergence Study

In finite element analysis, a more accurate solution is obtained from a finer mesh. However, a finer mesh also requires an increase in computational time. Therefore, a mesh convergence study was carried out to obtain a mesh that is a satisfactory balance of accuracy and available computing resources for the FEA. The mesh convergence study was done for both the ASTM and bus window pillar models to ensure that the element size is not too coarse.

3.2.5.1 ASTM Specimens

Figure 3-2-14 shows the mesh convergence curve of the ASTM model for the maximum principal stresses. The analysis was performed for the Maximum Principle Stresses for varying element size from 1 mm to 0.1mm. The number of elements increases from 10577 (at element size 1mm) to 451960 (at element size 0.1mm). The details of the element size and number of elements are shown at table A-3. After the mesh convergence, an element size of 0.1 mm was used as the optimum value.

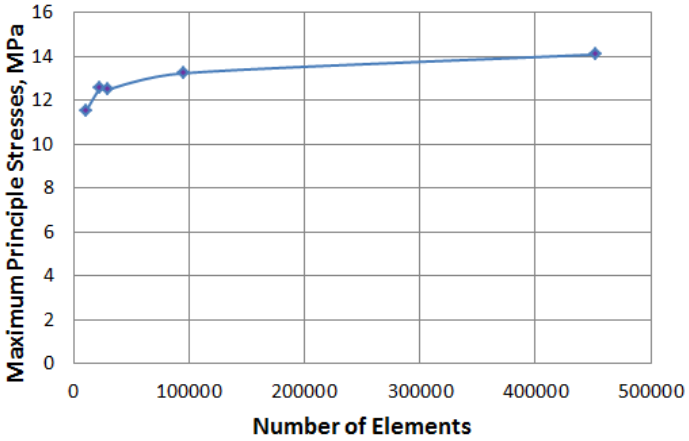

Figure 3- 2- 14 Mesh Convergence curve for the ASTM Model [41].

3.2.5.2 Bus Window Pillar

Figure 3-2-15 shows the mesh convergence curve of the bus window pillar for the von-Mises stresses. The analysis was performed for the Von-Mises Stresses for varying element size from 1 mm to 0.5mm. The number of elements increases from 79039 (at element size 1mm) to 766026 (at element size 0.5mm).

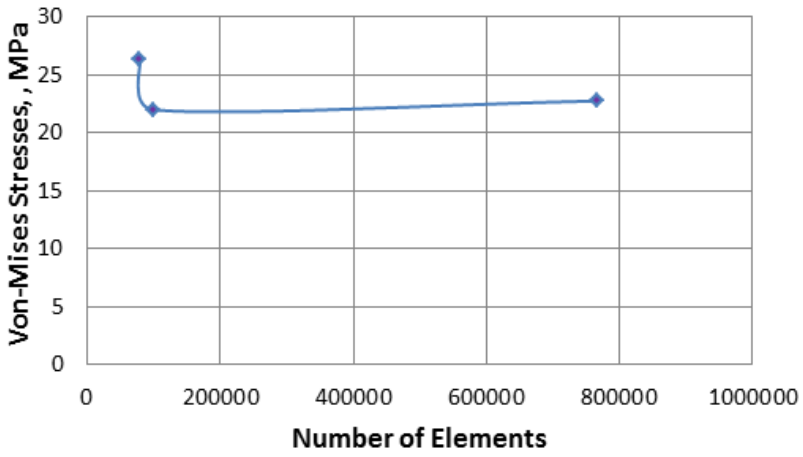

Figure 3- 2- 15 Mesh Convergence curve for the Bus window Pillar Model

3.3 Experimental Study

3.3.1 Tested Specimen

3.3.1.1 ASTM Specimens

The shape and dimensions of the tested specimen were formulated in accordance with the ASTM-E8 Standard Test Method for Tension Testing of Metallic Materials. The base material was SS 41003 and filler material was SS AWS ER 308L for the ASTM samples. These samples were prepared by the company of the bus window pillar. The dimensions of the specimens are shown in Fig. 3-3-1. The thickness of the samples is 3 mm.

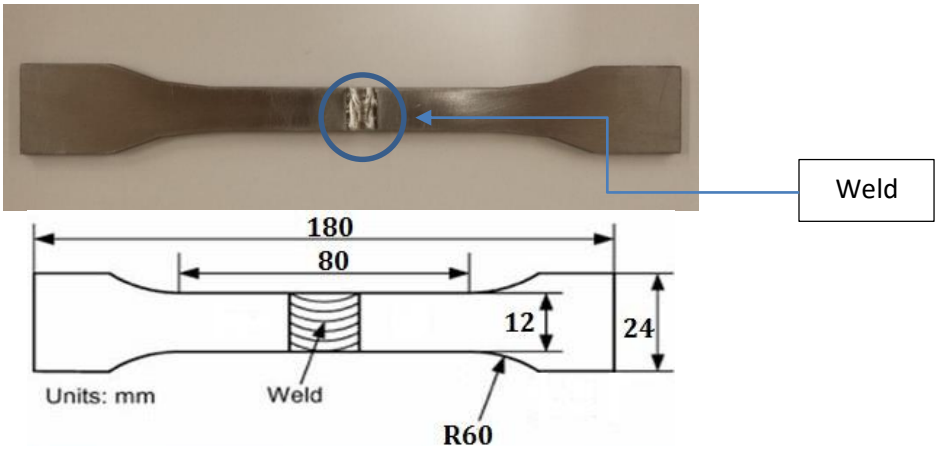

Figure 3- 3- 1 The shape and dimensions of ASTM welded sample

3.3.2 Strain Gage Attachments

Residual tensile stresses are found in weld metal and the section of the base metal that is adjacent to the weld zone or heat affected zone (HAZ) due to welding as shown in Fig. 3-3-3. Most of the failure occurs in the HAZ. It is not possible to directly place strain gages onto welds. Therefore, the strain gages were attached near the weld in the HAZ. In fact, the strain gages were attached 2-3 mm away from the weld in each sample.

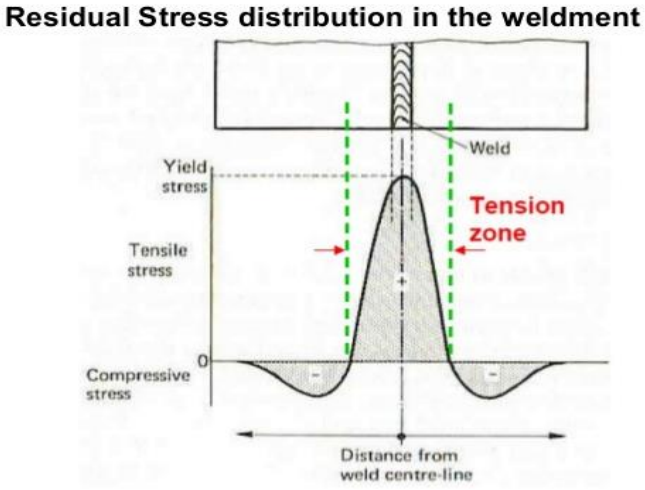

Figure 3- 3- 2 Residual tensile stresses exist in the weld metal and the adjacent base metal [43].

3.3.2.1 ASTM Specimens

As the width of the ASTM specimens is 6 mm, very small and precise strain gages were used for the testing. Due to size limitations, only one strain gage was attached onto each surface: one on the top surface and another on the bottom surface (Figure 3-3-4). Rectangular stacked rosette strain gages were used for the testing of the ASTM welded samples.

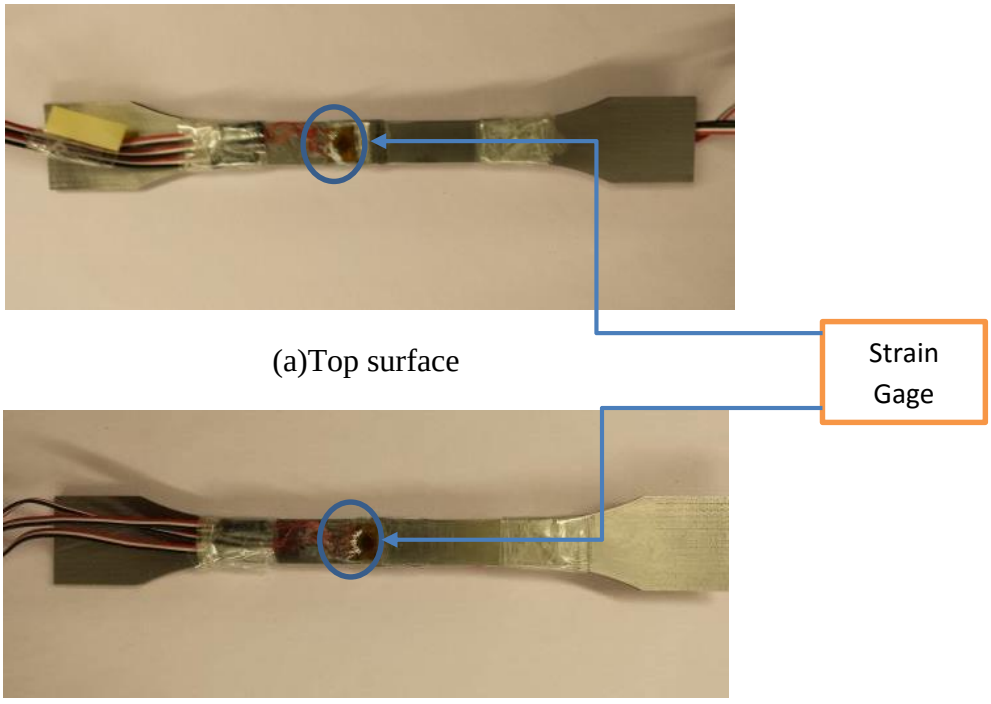

(a)Top surface

(b)Bottom surface

Figure 3- 3- 3 Strain gages attached on the ASTM sample [41].

3.3.3 Strain Gage Specifications

The specifications of the strain gages used are as follows. The model is C2A-06-125WW-350, and they are rectangular stacked rosette strain gages with 0°-45°-90° rosettes used in applications that involve limited gaging areas or steep strain gradients. The grid resistance (in ohms) is

350.0±0.6%, gage factor is 2.16 at 24°C, temperature range is -50°C to +66°C, and the strain range is 2%. The gage grid dimensions are 9.5×7.8 mm, and the active grid length is 3.18 mm.

3.3.4 Strain Gage Setup

A three-wire connection for a quarter-bridge strain gage circuit was used as the strain gage connection and shown in Fig. 3-3-6. The output of the strain gages and bridges are relatively small, which is less than 10 mV/V (10 mV of output per volt of excitation voltage). Therefore, an excitation voltage of 3.333 V per channel was used in the testing. This voltage excitation allows the amplifiers to boost the signal level to enhance measurement accuracy and make better the signal-to-noise ratio [44].

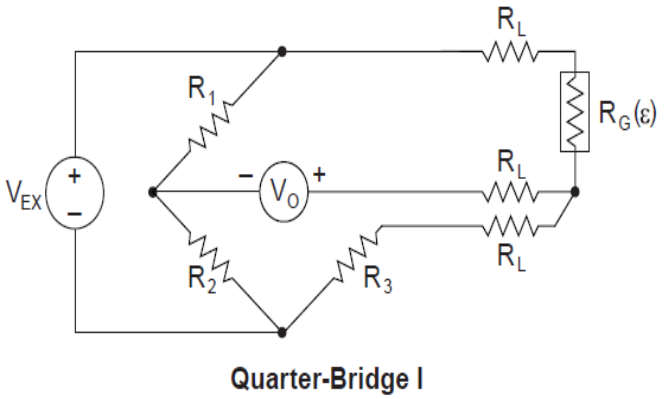

Figure 3- 3- 4 Three-Wire Connections of Quarter-Bridge I Circuit [44].

The main governing equation for calculating the strain is given below [44]:

$$\text{Strain } (\varepsilon) = \frac{-4V_r}{GF(1+2V_r)}\left(1+\frac{R_L}{R_G}\right) \qquad (4)$$

where, $V_r = \frac{V_{O(strained)} - V_{o(unstrained)}}{V_{EX}}$

R_G = nominal resistance value of the strain gage,

GF = gage factor of the strain gage, and

R_L = lead resistance.

3.3.5 Test Setup

Figure 3-3-7 shows the flow diagram of whole experimental setup for the testing of both the ASTM and bus window pillar samples. For the former, the IOtech data acquisition (DAQ) system is used to collect the data (physical changes) from the strain gages during testing. Then the DAQ sends the data to a laptop. The data are displayed and recorded by using the IOtech Encore software on the laptop. (Fig. 3-3-7). Fig. 3-3-8 shows the experimental setup of the testing of the ASTM samples. The testing was done at the materials testing facilities at the University of Manitoba. The test setup for the bus window pillar is the same. However, it was not possible to test the bus window pillar in the university lab due to its size. Instead, it was tested at the International Technology Center (ITC), where a large material testing machine (MTS) was used and a SOMAT DAQ system which simultaneously collected data from six strain gages.

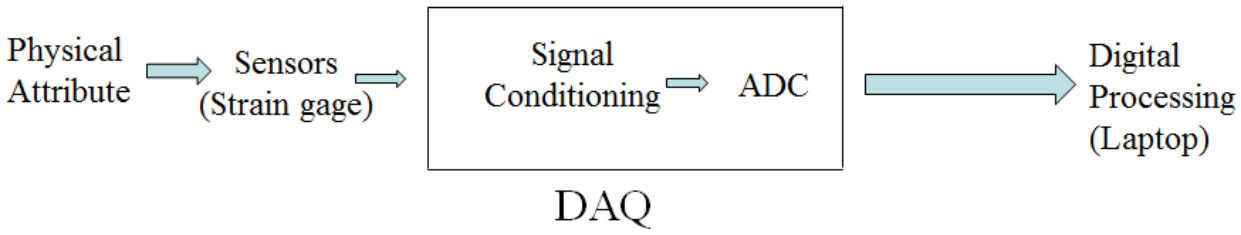

Figure 3- 3- 5 Experimental Test Setup [41].

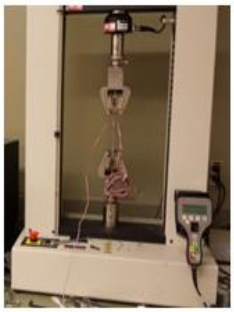

MTS Material Testing Machine

Iotech DAQ

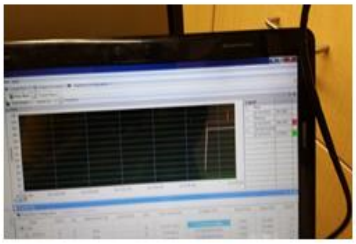

IOtech Encore

Figure 3- 3- 6 Experimental Setup for ASTM Specimen (Lab support: Material Testing Lab (E1-470)) [41].

During each timed load application, shunt calibrations between two points were carried out. The purpose of shunt calibrations is that it is a procedure used to compare the outputs of the strain gage measurement with a determined mechanical input or strain to verify the accuracy of the strain gage. This involves the simulation of the strain input which is done by varying the resistance of an arm in the bridge by a predetermined value.

3.3.6 Testing Procedure

3.3.5.1 ASTM Specimens

The static loading testing of the ASTM specimens was performed on an MTS machine (capacity of 30 kN) in a material testing lab at the University of Manitoba. One end of the ASTM specimen was fixed and a simple axial load (tension) was applied onto the other end (Figure 3-3-10). All of the ASTM specimens were tested under loads of 250 N, 500 N, 750 N, 1000 N, 1250 N, and 1500 N twice. The strain rate was 1 mm/min. For each load, testing was carried out 3-5 times to collect the data.

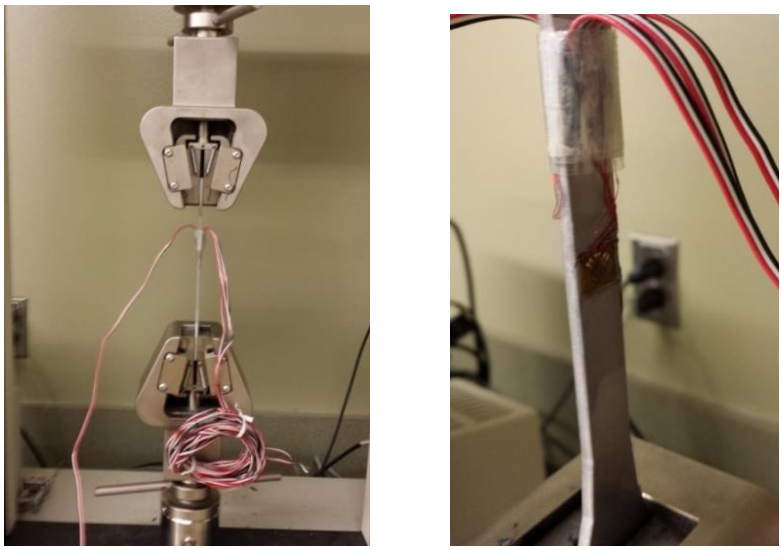

Figure 3- 3- 7 Testing of ASTM Specimen

3.4 Strain Gage Rosettes and Stress Calculation

Rectangular stacked rosettes were used in the experimental study. Historically, rectangular rosettes were more popular and calculations were much easier than with the use of other types of strain gages. The advantages of using strain gage rosettes are that they are suitable for determining multiaxial strain fields and different strain and stress fields for comparison with simulations [45], [46]. However, the advantages of rectangular stacked rosettes are that only a small surface area is required, they overcome the problem of large strain gradients and there is the same transverse sensitivity coefficient for all 3 arms [44], [45].

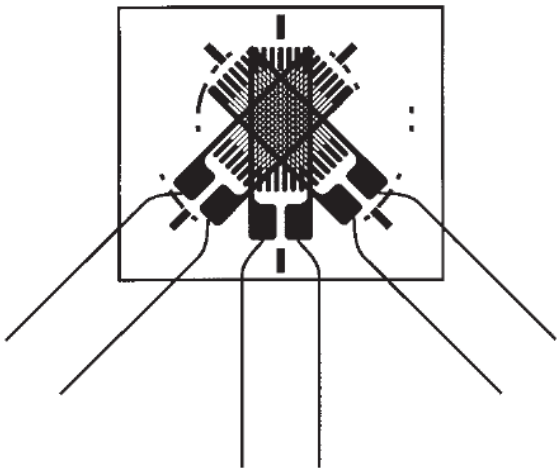

Figure 3- 4- 1 Rectangular rosettes in planar stacked construction [45].

3.4.1 Strain and Stress Measurement:

Strain gage rosettes are used where the principal strains and their direction are unknown. The principal strains can be calculated from the strain measurements of three rosette types of strain gages. The equations are derived from a "strain-transformation" relationship.

The expression of normal strain at any arbitrary angle θ from the major principal axis is [47], [48]:

$$\varepsilon_\theta = \frac{\varepsilon_x + \varepsilon_y}{2} + \frac{\varepsilon_x - \varepsilon_y}{2} cos2\theta + \frac{\gamma_{xy}}{2} sin2\theta \quad (5)$$

Consider a strain rosette attached to a surface at an angle of θ from the *x*-axis. With the use of a 0°-45°-90° rectangular rosette, internal angles of θ, θ+45° and θ+90° are found in the three strain gages as illustrated in Fig. 3-4-2.

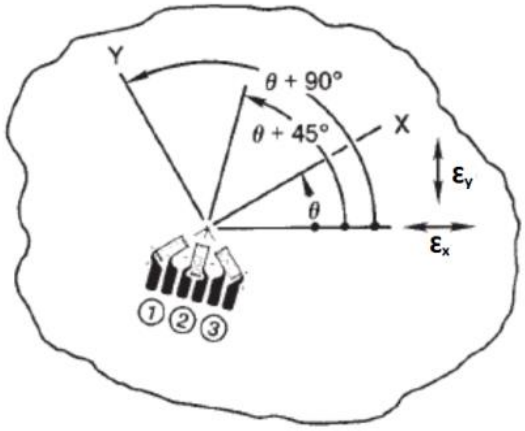

Figure 3- 4- 2 Rectangular rosette installed on a test surface, with Grid 1 at the arbitrary angle θ from the x- axis [45].

Assume that ε_a, ε_b, and ε_c are the strain measured from these three strain grids of the strain rosette respectively.

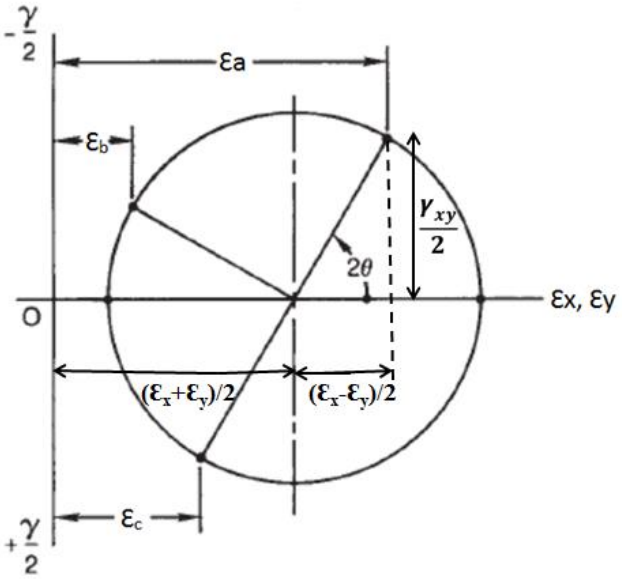

Figure 3- 4- 3 The axes of the rectangular rosette superimposed on Mohr's circle for strain.

The normal strains are calculated from the following strain transformation equations. The strain from each strain grid of the strain rosette is expressed in the *x-y* coordinates. The sensed strain by each grid can be written by the successive substitution of the angles for the three grid directions into Equation (5):

$$\varepsilon_a=\frac{\varepsilon_x+\varepsilon_y}{2}+\frac{\varepsilon_x-\varepsilon_y}{2}cos2\theta+\frac{\gamma_{xy}}{2}sin2\theta \quad 6(a)$$

$$\varepsilon_b=\frac{\varepsilon_x+\varepsilon_y}{2}+\frac{\varepsilon_x-\varepsilon_y}{2}cos2(\theta+45°)+\frac{\gamma_{xy}}{2}sin2(\theta+45°) \quad 6(b)$$

$$\varepsilon_c=\frac{\varepsilon_x+\varepsilon_y}{2}+\frac{\varepsilon_x-\varepsilon_y}{2}cos2(\theta+90°)+\frac{\gamma_{xy}}{2}sin2(\theta+90°) \quad 6(c)$$

The successive substitution of the angles for the three grid directions into Equation (6) means that these equations can be solved for the strains in the x-y system:

$$\varepsilon_x=\varepsilon_a+\varepsilon_c-\varepsilon_b \quad 7(a)$$

$$\varepsilon_y=\varepsilon_b \quad 7(b)$$

$$\gamma_{xy}=\varepsilon_a-\varepsilon_c \quad 7(c)$$

The largest normal strain, generally of most interest, is obtained by taking a derivative of the ε_θ strain (Equation (5)) with respect to θ and equating it to zero, which provides the principal rotation angle, θ_p that will produce the principal (maximum and minimum) strains. The resulting equations are [49]:

$$\tan 2\theta_p=\frac{\gamma_{xy}}{\varepsilon_x-\varepsilon_y} \quad 8(a)$$

$$\varepsilon_{1,2}=\frac{\varepsilon_x+\varepsilon_y}{2}\pm\sqrt{\left(\frac{\varepsilon_x-\varepsilon_y}{2}\right)^2+\left(\frac{\gamma_{xy}}{2}\right)^2} \quad 8(b)$$

These strains, ε_1 and ε_2, are called the principal strains.

The principal stresses can be determined from the principal strain values through the use of the following generalized Hooke's Law stress-strain relationship [49]:

$$\sigma_1 = \frac{E}{1-\upsilon^2}(\varepsilon_1 + \upsilon\varepsilon_2) \quad 9(a)$$

$$\sigma_2 = \frac{E}{1-\upsilon^2}(\varepsilon_2 + \upsilon\varepsilon_1) \quad 9(b)$$

The von-Mises stress for a plane stress element is calculated from the principal stress with the following equation [49]:

$$\sigma_{vm} = \sqrt{\frac{(\sigma_1-\sigma_2)^2+(\sigma_1)^2+(\sigma_2)^2}{2}} \quad (10)$$

3.5 Extracting Stresses

For stress comparison between the FEM and experimental results, the exact position of the strain gages was needed so that an accurate comparison between the stress values of the FEM model with the experimental results could be carried out. It was straightforward for the ASTM specimens because only one strain gage was attached onto each surface and the specimens have a regular geometry. Slide callipers were used to directly measure the position of the strain gage matrix. Since the bus window pillar has an irregular and complicated geometry, a special software, PIXEL Ruler, was used to measure the position of the strain gages. A picture of the strain gage plane was taken with a ruler on the surface, which was used to calibrate the distance with the software and then the exact positions of the strain gages were measured. The link element/ path was placed into the FEM model on these measured positions from the software.

The exact same boundary conditions were applied and then the stresses extracted from the link element/ path of the FEM model for comparison with the experimental results.

Chapter 4 Results and Discussion

4.1 ASTM Specimens

4.1.1 Stress Analysis of ASTM Model

The ASTM specimens were modeled and analyzed by using the effective notch stress method in ANSYS Workbench. Figure 4-1-1 shows the three different types of stress distributions in the ASTM specimens under a load of 250 N. The stress distribution behaviors are almost the same but the magnitude of the stress values is different. The maximum principal stresses are greater for this axial load. The maximum von-Mises stresses are slightly lower than the maximum principal stresses. There is also the presence of shear stresses in the base metal area adjacent to the welded area. The maximum shear stresses are slightly lower than half of the maximum principal stresses.

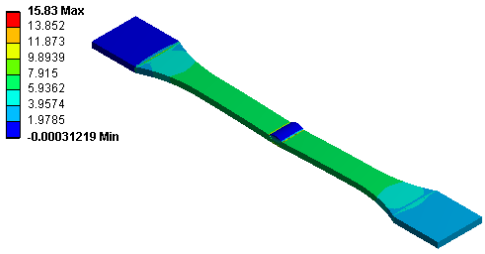

(a) Principal Stresses distribution

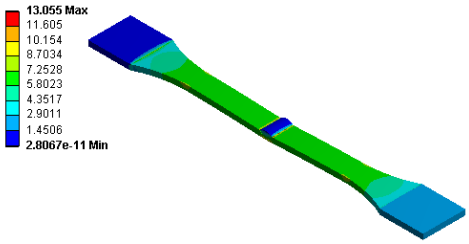

(b) Von-Mises Stresses distribution

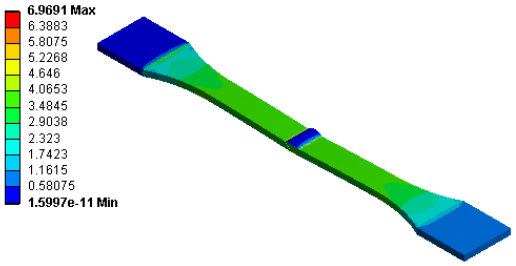

(c) Shear Stresses distribution

Figure 4- 1- 1 Stresses distribution in the ASTM FEM model at 250N

In practice, welding gives rise to internal tensile stresses adjacent to the weld area. During loading, this area is subjected to higher stresses than the base metal area. This weld model that is based on the effective notch stress approach can simulate the stress distribution around the weld. Figure 4-1-2 shows that the maximum principal stresses occur at the weld toe. Figure 4-1-3 shows the maximum principal stress distribution along the longitudinal direction of the specimen.

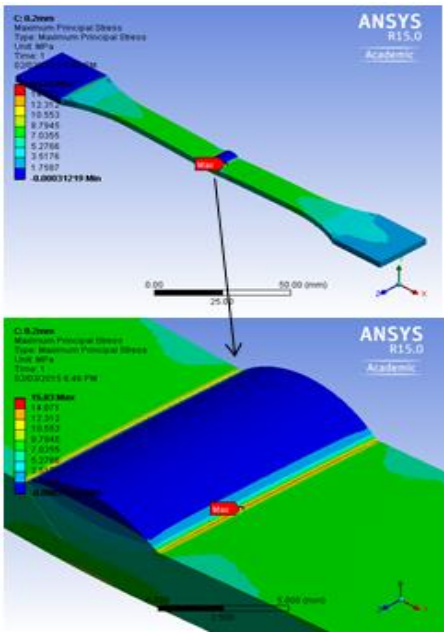

Figure 4- 1- 2 Maximum Principal Stresses occurs in the weld toe [41].

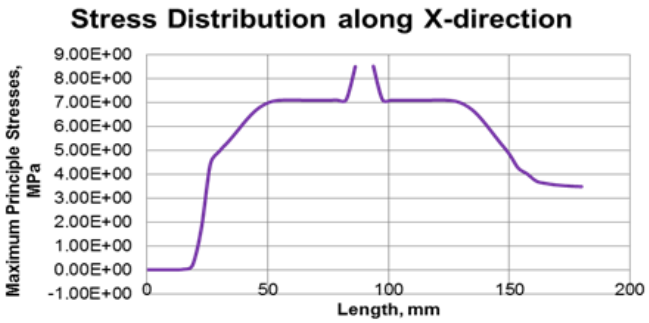

Figure 4- 1- 3 Maximum Principal Stress distribution along the X-direction of the specimen [41].

4.1.2 Effective Notch Radius Tuning and Experimental Validation

Parameter tuning in an FE model is very important for cross validation with the experimental results. During cross validation, the value of a selected parameter is chosen from several probable values of that parameter. This value yields the minimum cross-validation error and then that value is used to finalize the modeling. For this weld model, the effective notch radius is the only tuning parameter. The model was tuned with several values of the effective notch radius for cross validation. Figure 4-1-4 shows the tuning of an effective notch radius of 0.1 mm, 0.2 mm, 0.3 mm, 0.4 mm and 0.5 mm under five different loading conditions for the maximum principal stresses. Moreover, Fig. 4-1-4 indicates that the maximum principal stresses are sensitive to the effective notch radius. The decrease in the size of the notch radius will increase the maximum principal stresses. For example, under a load of 500 N, the maximum principal stresses are 26.5 MPa, 27.2 MPa, 29.4 MPa, 31.7 MPa and 41.6 MPa for a notch radius of 0.5 mm, 0.4 mm, 0.3 mm, 0.2 mm, and 0.1 mm respectively.

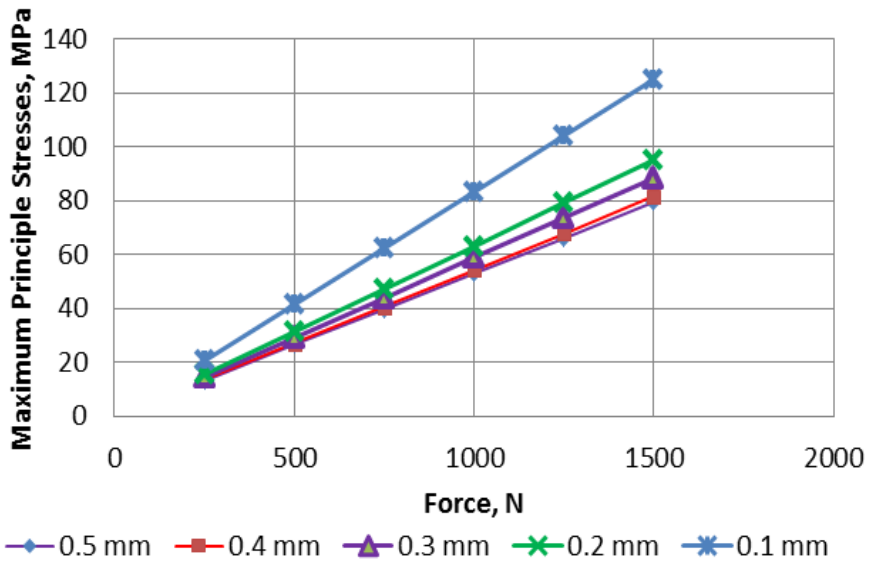

Figure 4- 1- 4 Tuning of Effective Notch Radius [41].

Force, N	Maximum Principal Stresses, MPa
250	9.87

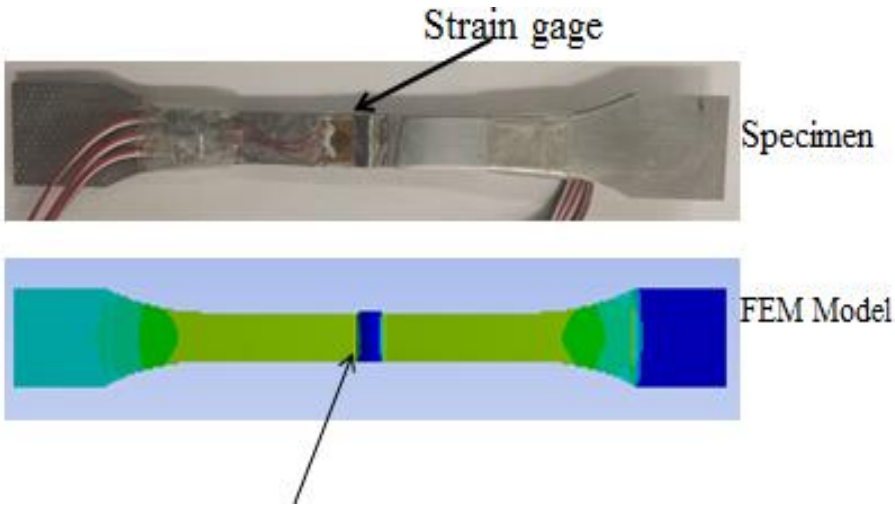

Force, N	Notch Radius, mm				
	0.5	0.4	0.3	0.2	0.1
	Maximum Principal Stresses, MPa				
250	8.77	9.13	9.60	9.82	10.24

Figure 4- 1- 5 Comparison of Actual specimen and FEM Model [41].

The maximum principal stresses under a load of 250 N as determined by the strain gages were used in the cross-validation of the ASTM specimens. The strain gages were attached 2-3 mm away from the weld. For cross validation, the maximum principal stresses were obtained from the same location as the FEM model where the strain gages were attached on the actual ASTM specimens. The link element that had the same size as the strain gages was used in the FEM model. The link element behaves like the strain gages and was placed in the same location where the strain gages were attached onto the ASTM specimens (Figure 4-1-5) [41].

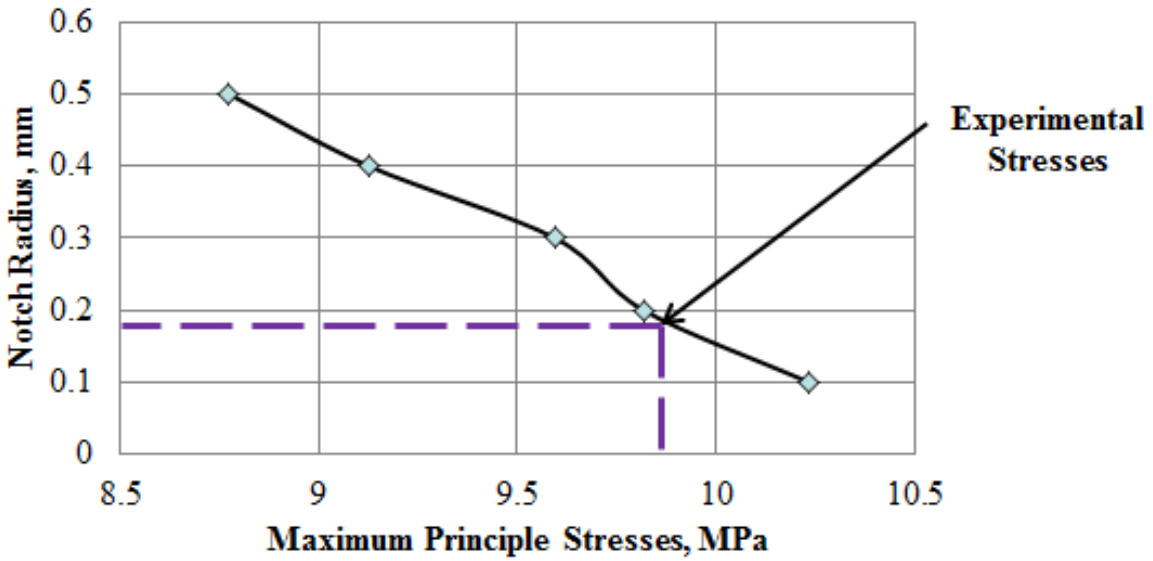

Figure 4- 1- 6 Tuning of FEM Model and Cross [41].

The maximum principal stresses of the link element under a load of 250 N were then compared with the experimental results obtained by using the strain gages. As shown in Figure 4-1-6, the maximum principal stresses are reduced as the effective notch radius is increased under a load of 250 N. The testing results agree with the FEM results when the effective notch radius value is close to 0.2 mm. This is the optimum value of the effective notch radius for this model. This value corresponds to the minimum validation error for the ASTM specimens.

4.1.3 Experimental Validation of Misaligned ASTM Samples

In this study, it is found that an effective notch radius that is close to 0.2 mm gives the lowest validation error in the experiment with the ASTM samples. Aside from that, some of the ASTM specimens have axial misalignment under the same loading conditions. Therefore, welded specimens with misalignment and exactly the same geometry of the misaligned ASTM specimens were developed by using the FEM in ANSYS. The optimum value of the effective notch radius, which is 0.2 mm, and an element size of 0.1 mm were used. Then the FEM and

experimental results were compared for cross validation. A close approximation was found between the two results, and the difference between them is 5-10%. Figure 4-1-7 shows a comparison of the maximum principal stresses between the FEM and experimental results of the misaligned specimens.

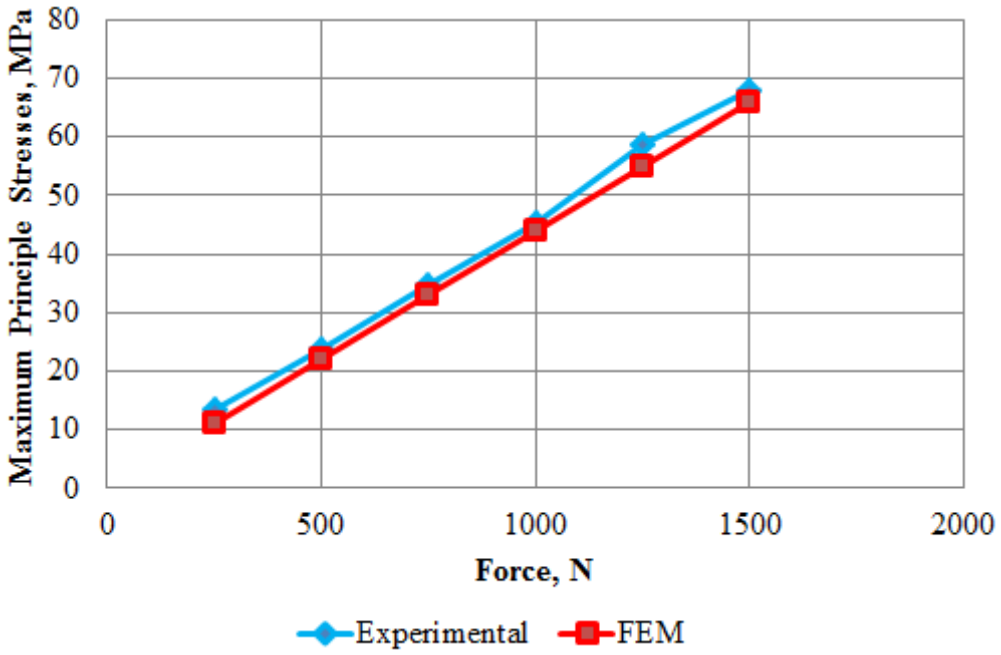

Figure 4- 1- 7 Comparison of Maximum Principal stresses between misaligned FEM and Experimental results [41].

4.1.4 Stress Analysis of Normal and Misaligned ASTM Specimens

Both normal and misaligned ASTM specimens were tested. However, there is axial misalignment in the latter, which causes deterioration and gives rise to bending stresses adjacent of the weld. Consequently, the stress distribution becomes more complicated around the weld. The axial and bending stresses contribute to the total stress on a misaligned welded joint. The axial misalignment of the misaligned specimens in this study is approximately 0.45-0.5 mm, or

about 20% of their thickness. The maximum principal stresses between the misaligned and normal welded specimens are compared with the strain gages. It was found that an axial misalignment of 20% of the specimen thickness increases the maximum principal stresses by 25%-35%. Figure 4-1-8 shows a comparison of the maximum principal stresses between the misaligned and normal welded specimens.

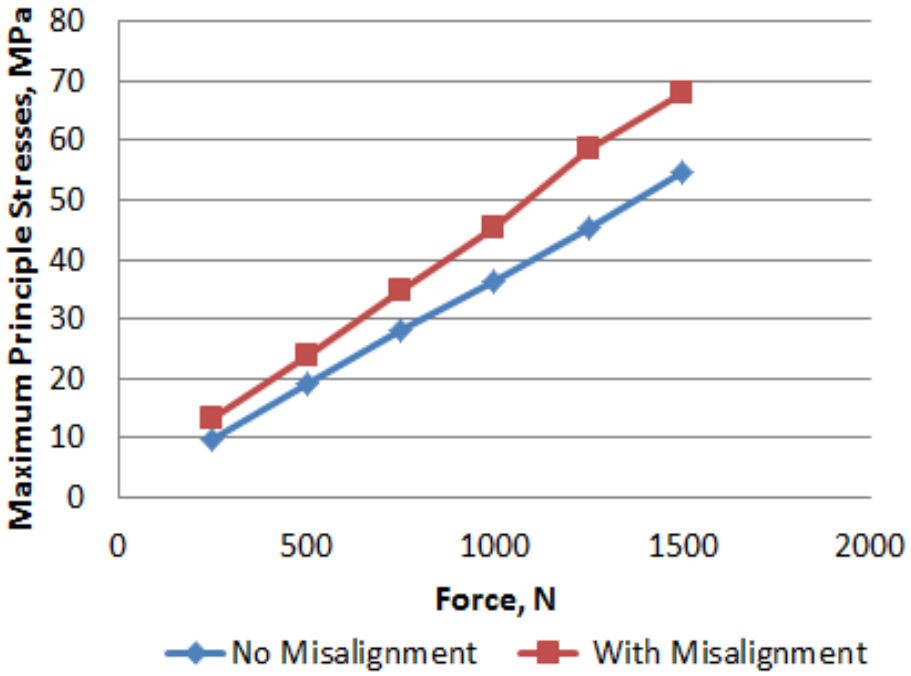

Figure 4- 1- 8 Experimental Results of welded specimen (Misalignment vs. No-misalignment) [41].

4.1.5 Effects of Misalignment

The weld model with an optimum effective notch radius of 0.2 mm was analyzed with different values of axial misalignment from no misalignment to 0.75 mm of axial misalignment in ANSYS Workbench. Figures 4-1-9 (a) and (b) show the maximum principal and maximum shear stresses at different values of axial misalignment on the FE welded specimens. Both the maximum principal and maximum shear stresses increase with an increase in axial misalignment.

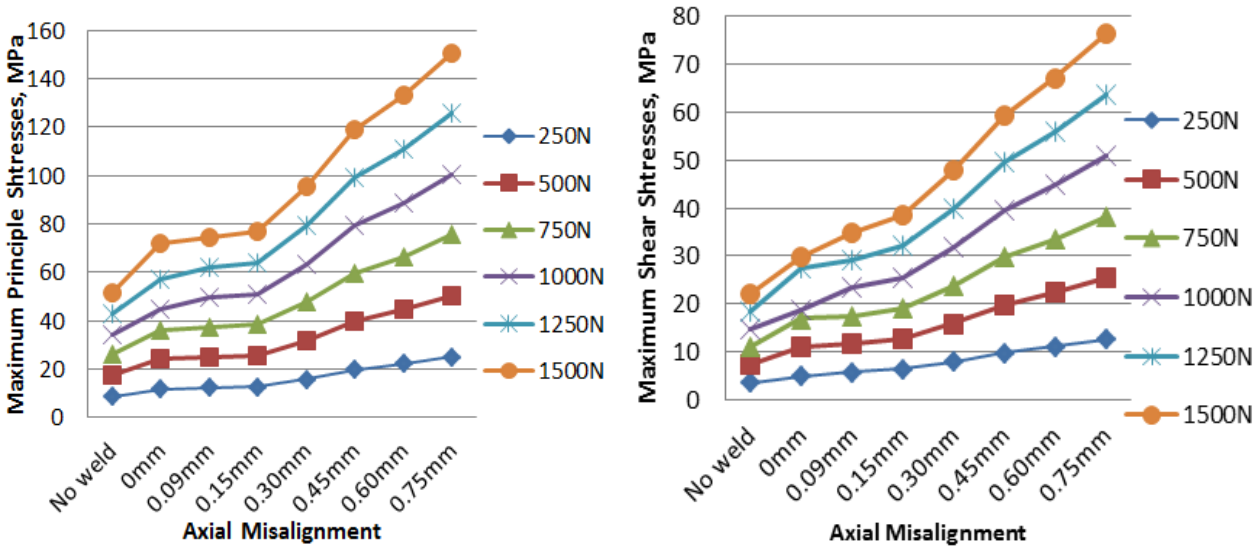

(a) (b)

Figure 4- 1- 9 Effect of axial misalignment on (a) Maximum Principal Stresses and (b) Maximum Shear Stresses [41].

4.2 Bus Window Pillar

4.2.1 Stress Analysis of Bus Window Pillar

Finite-element models of the bus window pillar were developed to study the structural behavior and stress fields near the weld joints. The effective notch stress method was also used to evaluate the local stresses at the toe of the welded joint and for experimental validation. The window joint was analyzed for only one standard loading case. Figure 4-2-1 shows the maximum principal strains and maximum shear strain distribution on the window pillar joint under the same loading condition.

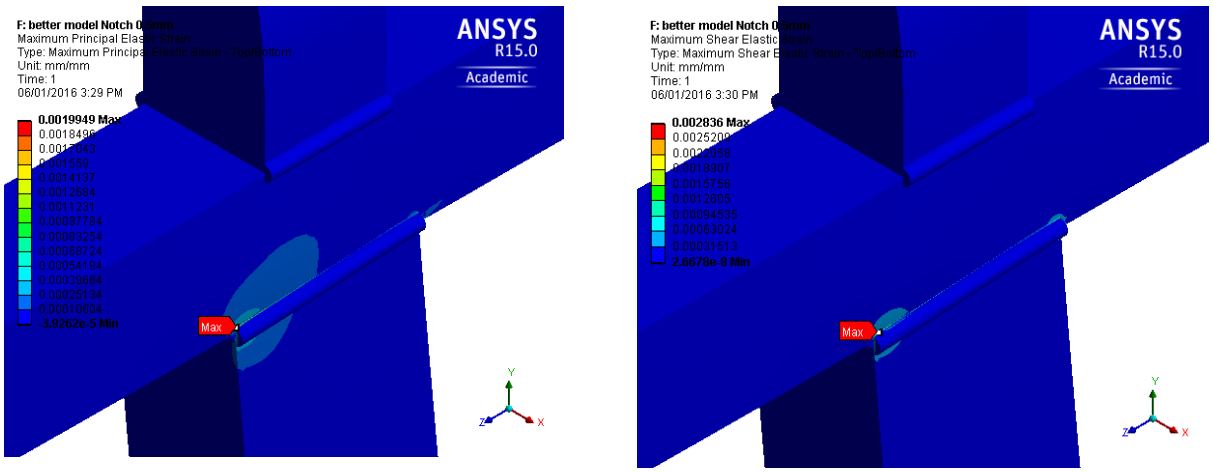

(a) Maximum Principal Elastic Strains **(b)** Maximum Shear Strains

Figure 4- 2- 1 Strain distribution in Finite Element Window Pillar Model

As shown in both plots in Fig. 4-2-1, high elastic strains are distributed in the adjacent area of the welding (near the weld toe zone). The simulation by using FEM shows that the strains propagate from the left corner surface all the way to the mid-surface and then to the right. The actual failure also occurred in the same manner in the practical field.

The magnitude of the maximum shear strains is greater than that of the maximum elastic principal strains at the critical locations. However, the magnitude of the maximum principal stresses is almost double that of the maximum shear stresses at the critical locations. This can be explained by local bending due to the increased deterioration in the critical locations during standard loading. Figure 4-2-3 shows the maximum principal and maximum shear stress distributions on the window pillar joints under the same loading condition.

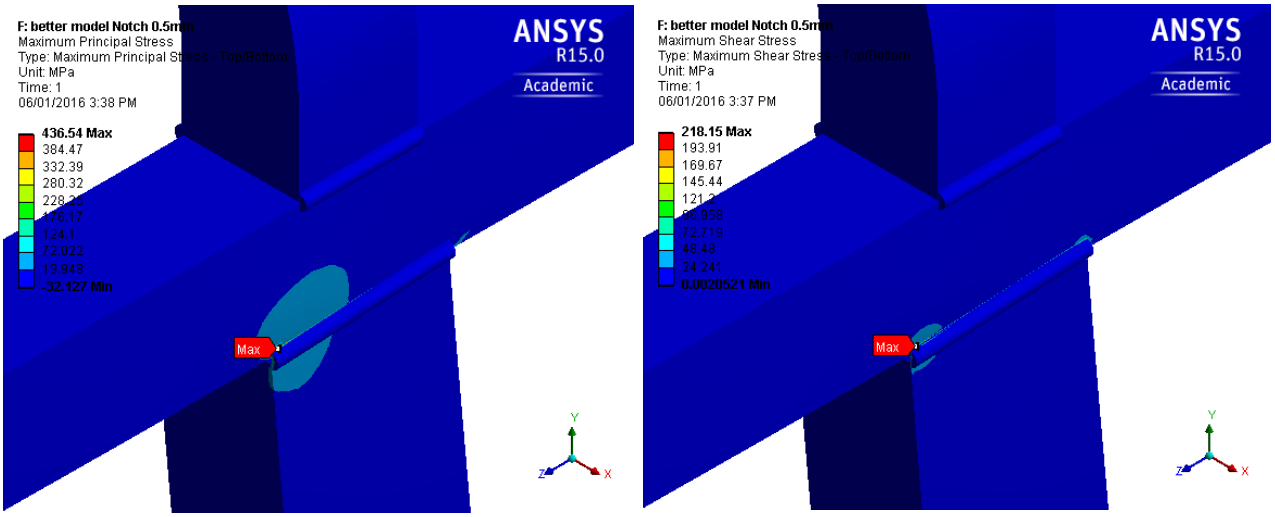

(a) Maximum Principal Stresses (b) Maximum Shear Stresses

Figure 4- 2- 2 Stress distribution in Finite Element Window Pillar Model

At the critical locations, the maximum principal stresses as well as a large amount of maximum shear stresses were found. Thus, a combination of solid and shell elements was used for the finite element modeling of the bus window pillar. The von-Mises stress is an appropriate stress criterion for the stress analysis of the complex structure of the bus window pillar. von Mises stresses provide all six stress components of a general 3-D state of stress. The von Mises criterion is usually used for ductile materials, like steel, aluminum, most plastics, etc. Figure 4-2-4 shows the von-Mises stress distribution on the window pillar joint. The maximum von-Mises stresses are found at the weld toe. The von-Mises stresses are higher at the adjacent area of the welding which has the same distribution pattern as the maximum principal and maximum shear stresses.

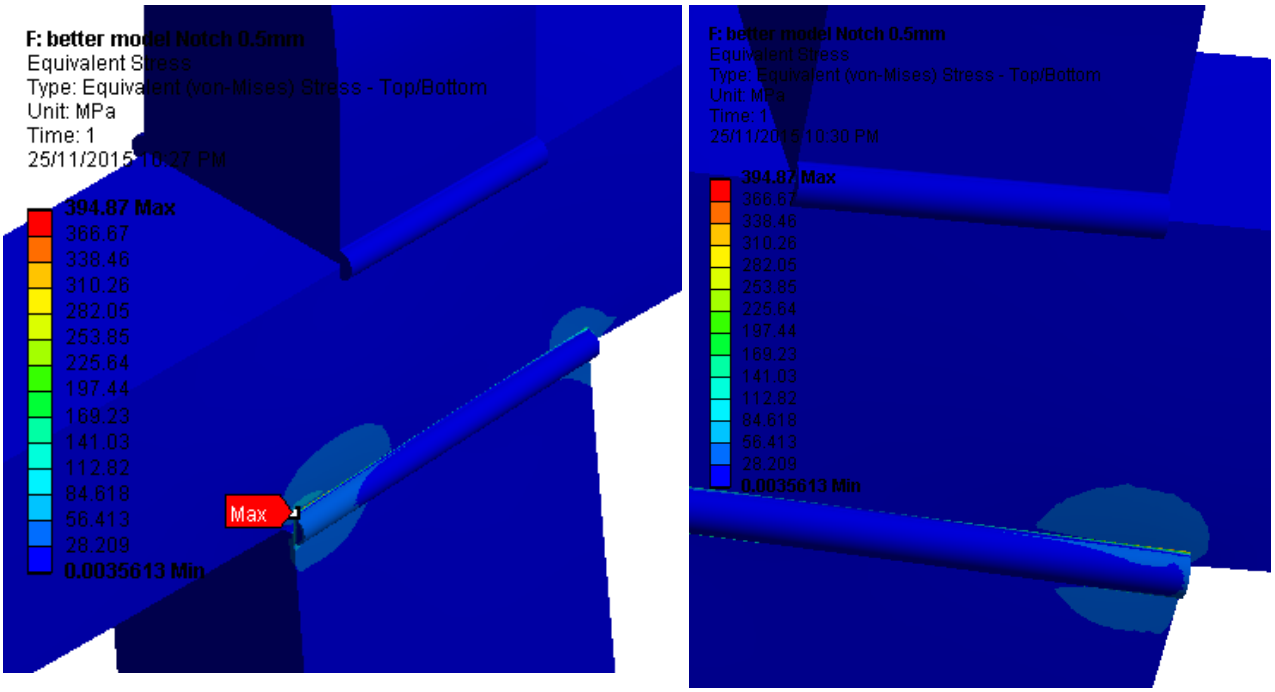

Front View **Rear View**

Figure 4- 2- 3 Von-Mises Stress Distribution in Finite Element Model of the Window Pillar

4.2.3 Experimental Validation for Bus Window Pillar

The window pillar model is very large and complex compared with the ASTM model. The FEM results of the window pillar were simultaneously compared with the experimental results for all the strain gages at different notch radius. It was significantly challenging to match the FEM results with all the strain gages. For comparison purposes, the same procedure used for the ASTM specimens was followed, which was discussed in Section 4.1.2. A good and consistent agreement was found between the experimental and the FEM results for the bus window pillar model. The details experimental validation of the bus window pillar is not included in this thesis due to the confidentiality agreement.

Chapter 5 Conclusions

In this research work, two different types of welded joints are investigated. They are evaluated by using a FEM model with the effective notch stress approach which is compared with the experimental results. The following summary is based on this analysis.

- The modelling technique (effective notch radius tuning) proposed in this paper can provide better results for complicated stress fields, when the possible singularities near the critical areas are avoided. This model can differentiate whether the critical location is at the weld toe or the weld root. This technique can also be applied to complex geometries. So far, the results have been encouraging for both the ASTM and window pillar specimens.

- The FEM results show good agreement with the experimental results (obtained by using strain gages) for the ASTM specimen with an effective notch radius that is approximately 0.2 mm. This reference radius has been successfully used in the experimental validation of the misaligned ASTM specimen.
- Axial misalignment increases the total stress adjacent to the welded area. The axial misalignment of 20% of the thickness of the specimens would have increased over 30% of the maximum principal stresses on the ASTM specimens.
- The bus window pillar model shows a very good agreement with the experimental results for most of the strain gages under different loading points at optimum effective notch raidus.

- In terms of the FEM model of the bus window pillar, the maximum notch stress occurs at the weld toe on the bottom welded part of the top surface. This indicates that cracks are more likely to propagate into the HAZ to the weld metal. This is also showing a good agreement with the actual observed crack pattern of the bus window pillar. Therefore, the effective notch stress approach is a good means to simulate the observed crack patterns.
- Based on the experience obtained from the modelling efforts in this study, the effective notch stress method is considered to be suitable for the stress analysis of simple as well as complicated structures.

Chapter 6 Future Works

The following are some recommendations for future work based on this study.

The effective notch stress approach is a relatively new approach in weld modeling. This research is one of the first attempts to validate a weld model by tuning the effective notch radius. In all of the previous studies, an absolute value of the effective notch radius is used for modeling based on the thickness of the welded plate. Therefore, more research is required to confirm the accuracy of the method and techniques.

Fillet welded joints normally fail at the weld toe. In this research, welded joints are modeled by considering the weld toe failure. This weld model which uses the effective notch stress approach can be validated for other types of welded joints to examine weld root failure.

In this research, only two different types of specimens are investigated with the use of the effective notch stress approach for experimental validation. Each specimen is subjected to only one type of loading condition. The developed FE model can also be verified by using different variables, such as different geometries, materials, boundary conditions, etc.

The majority of published studies have focused on simple geometries. However, a complicated geometry (window pillar) has been examined in this work. More research is therefore required on advanced geometries in order to obtain a better understanding of the application of the effective notch stress approach.

The experimental von-Mises stresses of the HAZ are calculated from principal strains that use the elasticity of modulus of the base metal. The material properties (E, υ, etc.) of the HAZ need to be measured for more accurate experimental validation. In the next phase of this research,

there are plans to use the digital image correlation (DIC) technique and ULTRA MARS tool to measure the material properties of HAZs.

This modeling technique which uses the effective notch radius does not rely on the weld size. Therefore, it can be useful for studying weld models with various weld sizes under different loading conditions. The results from such a study might be helpful for determining the relationship between the effective notch radius and weld size.

In terms of the bus window pillar modeling, the difference between the FEM and experimental results is around 10-15%. The tuning of the notch radius is limited by the software license and post-processing resources. This model can therefore be refined and better analyzed by using WESTGRID processors.

References

[1] Wikipedia, “Structural integrity and failure,” 2012. [Online]. Available: https://en.wikipedia.org/wiki/Structural_integrity_and_failure. [Accessed: 07-Jan-2015].

[2] Fikssan, “Bus Body Frame.” [Online]. Available: http://www.fikssan.com/EN/yetkinliklerimiz1.aspx. [Accessed: 09-May-2016].

[3] W. Fricke, “Fatigue analysis of welded joints: State of development,” *Mar. Struct.*, vol. 16, no. 3, pp. 185–200, 2003.

[4] M. Aygul, “Fatigue Analysis of Welded Structures Using the Finite Element Method,” 2012.

[5] M. Heshmati, “Fatigue Life Assessment of Bridge Details Using Finite Element Method,” pp. 1–272, 2012.

[6] a. Hobbacher, “Recomendation for Fatigue Design of Welded Joints and Components,” *IIW Doc. IIW-1823-07 ex XIII-2151r4-07/XV-1254r4-07*, 2008.

[7] S. S. Karganroudi, “Fatigue study of the fillet weld waving on weld toe and the penetration in the weld root based on the effective notch stress approach,” 2012.

[8] W. Fricke and H. Petershagen, “Detail Design of Welded Ship Structures Based on Hot-Spot Stresses,” in *Practical design of welded ships and mobile units*, 1992, pp. 21087–21100.

[9] D. Radaj and M. Vormwald, *Advanced Methods of Fatigue Assessment*. 2013.

[10] E. Niemi, *Stress Determination for Fatigue Analysis of Welded Components*. Woodhead Publishing Limited, 1995.

[11] S. Technology and B. J. Leira, “Approaches for assessment of weld fatigue and verification of the effective notch stress approach Øyvind Sæbø Fagnastøl,” no. June, 2014.

[12] M. Malikoutsakis and G. Savaidis, “Modeling and fatigue assessment of weld start-end

locations based on the effective notch stress approach," *Materwiss. Werksttech.*, vol. 42, no. 4, pp. 298–305, 2011.

[13] C. M. Sonsino, W. Fricke, F. De Bruyne, a. Hoppe, a. Ahmadi, and G. Zhang, "Notch stress concepts for the fatigue assessment of welded joints - Background and applications," *Int. J. Fatigue*, vol. 34, no. 1, pp. 2–16, 2012.

[14] D. Radaj, P. Lazzarin, and F. Berto, "Generalised Neuber concept of fictitious notch rounding," *Int. J. Fatigue*, vol. 51, pp. 105–115, 2013.

[15] D. Radaj, C. M. Sonsino, and W. Fricke, "Recent developments in local concepts of fatigue assessment of welded joints," *Int. J. Fatigue*, vol. 31, no. 1, pp. 2–11, 2009.

[16] W. Fricke, A. Bollero, I. Chirica, Y. Garbatov, F. Jancart, A. Kahl, H. Remes, C. M. Rizzo, H. von Selle, A. Urban, and L. Wei, "Round robin study on structural hot-spot and effective notch stress analysis," *Ships Offshore Struct.*, vol. 3, no. 4, pp. 335–345, Dec. 2008.

[17] M. Kaffenberger and M. Vormwald, "Fatigue resistance of weld ends - Analysis of the notch stress using real geometry," *Materwiss. Werksttech.*, vol. 42, no. 10, pp. 874–880, 2011.

[18] H. Neuber, *Kerbspannungslehre*, 3rd editio. Berlin, Germany: Springer, 1985.

[19] H. Neuber, *Kerbspannungslehre*, 2nd editio. Berlin, Germany: Springer, 1958.

[20] H. Neuber, "Über die berücksichtigung der spannungskonzentration bei festigkeitsberechnungen," *Konstruktion*, vol. 20, no. 7, pp. 245–251, 1968.

[21] D. Radaj, *Design and Analysis of Fatigue Resistant Welded Structures*. Cambridge, UK: Abington, 1990.

[22] F. Berto, "A Brief Review of Some Local Approaches for the Failure Assessment of Brittle and Quasi-Brittle Materials," *Adv. Mater. Sci. Eng.*, vol. 2014, 2014.

[23] J. Schijve, "Fatigue predictions of welded joints and the effective notch stress concept," *Int. J. Fatigue*, vol. 45, pp. 31–38, Dec. 2012.

[24] W. Fricke, “Round-Robin Study on Stress Analysis for the Effective Notch Stress Approach,” *Weld. World*, vol. 51, no. 3–4, pp. 68–79, 2013.

[25] W. Park and C. Miki, “Fatigue assessment of large-size welded joints based on the effective notch stress approach,” *Int. J. Fatigue*, vol. 30, no. 9, pp. 1556–1568, 2008.

[26] N. L. Pang;, X. L. Zhao;, F. R. Mashiri;, P. Dayawansa;, and J. W. H. Price, “design of welded thick-walled tubular dragline joints using 2D effective notch stress method (2).pdf.” International Journal of Steel Structures, pp. 279–288, 2006.

[27] C. Morgenstern, C. M. Sonsino, a. Hobbacher, and F. Sorbo, “Fatigue design of aluminium welded joints by the local stress concept with the fictitious notch radius of rf=1 mm,” *Int. J. Fatigue*, vol. 28, no. 8, pp. 881–890, 2006.

[28] M. Malikoutsakis and G. Savaidis, “an Approach To the Effective Notch Stress Concept To Complex Geometry Welds Focusing on the Fe Modeling,” 2009.

[29] S. Maljaars, W. Van Den Bos, M. Bloem, and J. C. Rijsenbrij, “Application of the fictitious notch stress approach and comparison with other stress based approaches.”

[30] H.-B. Sim, “Effective Notch Stress Method for Fatigue Evaluation of Welded Joints in a Steel Bridge Deck,” vol. 5, no. 2, pp. 89–92, 2012.

[31] M. M. Pedersen, O. O. Mouritsen, M. R. Hansen, J. G. Andersen, and J. Wenderby, “Re-analysis of fatigue data for welded joints using the notch stress approach,” *Int. J. Fatigue*, vol. 32, no. 10, pp. 1620–1626, 2010.

[32] C. V. Dung, E. Sasaki, K. Tajima, and T. Suzuki, “Investigations on the effect of weld penetration on fatigue strength of rib-to-deck welded joints in orthotropic steel decks,” *Int. J. Steel Struct.*, vol. 14, no. 4, pp. 1–12, 2014.

[33] R. Smith, “Thirty years of fatigue crack growth—a historical review,” *Int. Fatigue Crack Growth*, vol. 21, no. 5, pp. 1–16, 1986.

[34] P. Paris, “Fracture mechanics and fatigue: a historical perspective,” *Fatigue Fract. Eng. Mater. Struct.*, vol. 21, no. 5, pp. 535–40, 1998.

[35] T. L. Anderson, *Fracture Mechanics: Fundamentals and Applications, Third Edition*. 2005.

[36] Z. Barsoum and I. Barsoum, "Residual stress effects on fatigue life of welded structures using LEFM," *Eng. Fail. Anal.*, vol. 16, no. 1, pp. 449–467, 2009.

[37] Z. Barsoum, "Residual stress analysis and fatigue of multi-pass welded tubular structures," *Eng. Fail. Anal.*, vol. 15, no. 7, pp. 863–874, 2008.

[38] J. Barsom, "Fatigue crack growth under variable amplitude loading in various bridge steels," *ASTM STP 595*, 1976.

[39] Wikipedia, "Finite element method," 2012. [Online]. Available: https://en.wikipedia.org/wiki/Finite_element_method. [Accessed: 01-Feb-2016].

[40] SAE, "Finite Element Analysis (FEA) for Design Engineers," 2016. [Online]. Available: http://training.sae.org/webseminars/wb1241/. [Accessed: 01-Feb-2016].

[41] M. Nuruzzaman, C. Q. Wu, and O. Ojo, "Modeling of Welding Joint using Effective Notch Stress Approach for Misalignment Analysis," 2015, pp. 1–8.

[42] ANSYS Inc., "ANSYS Mechanical Introduction to Structural Nonlinearities," 2013.

[43] N. Syahroni and M. I. P. Hidayat, "Numerical Simulation of Welding Sequence Effect on Temperature Distribution, Residual Stresses and Distortions of T-Joint Fillet Welds," *Adv. Mater. Process. Technol. II*, vol. 264–265, pp. 254–259, 2011.

[44] National Instruments, "Measuring Strain with Strain Gages," 2014. [Online]. Available: http://www.ni.com/.

[45] Vishay Precision Group, "Tech Note TN-515: Strain Gage Rosettes : Selection , Application and Data Reduction," no. c, pp. 151–162, 2010.

[46] V. P. Group, "General Purpose Strain Gages - Stacked Rosette."

[47] S. P. Gere, James M.; Timoshenko, *Mechanics Of Materials J M Gere And Timoshenko 3rd Edition*. PWS Publishing Company, 1990.

[48] O. a. Bachau and J. Craig, “Strain Transformation and Rosette Gage Theory. 2D Strain Transformation and Mohr’s Circle,” *Struct. Anal. With Appl. to Aerosp. Struct.*, vol. 2, no. 1, pp. 1–7, 2009.

[49] F. P. Beer, E. R. Johnston, J. T. DeWolf, and D. F. Mazurek, *Mechanics of Materials*, 6 th editi. Newyork: McGraw-Hill, 2011.

Appendix A Experimental Raw Data and FEM Calculations of ASTM Standard Specimen

Table A- 1 Mean Grid strains of Top Surface from the Strain Gages for all test runs

	SNEG45_1		S90_1		S45_1	
Force, N	Mean, με	Standard Deviation	Mean, με	Standard Deviation	Mean, με	Standard Deviation
250	20.15	2.96	47.01	2.81	14.10	3.29
500	37.56	3.20	90.66	5.34	25.66	4.47
750	57.11	5.09	133.45	4.72	36.31	8.72
1000	75.33	9.56	173.70	6.78	50.48	7.99
1250	93.60	12.86	215.94	7.43	68.14	9.40
1500	114.02	12.53	260.92	7.45	80.11	13.25

Table A- 2 Mean Grid strains of Bottom Surface from the Strain Gages for all test runs

	SNEG45_1		S90_1		S45_1	
Force, N	Mean, με	Standard Deviation	Mean, με	Standard Deviation	Mean, με	Standard Deviation
250	9.03	1.99	26.38	5.54	5.89	1.30
500	17.60	3.70	50.16	10.53	11.72	2.46
750	26.06	5.47	74.71	15.69	17.94	3.77
1000	34.10	7.16	99.80	20.96	23.31	4.90
1250	44.94	9.44	122.89	25.81	26.62	5.59
1500	54.27	11.40	147.35	30.94	30.22	6.35

Table A- 3 Mesh Convergence Study of ASTM Specimen

Element Size, mm	Number of Element	Maximum Principal Stresses, MPa
1	10577	11.54
0.8	12857	11.92
0.5	22771	12.36
0.4	29133	12.50
0.2	95038	13.24
0.1	451960	14.09

Table A- 4 Effective Notch Radius Tuning

Force, N	Notch Radius, mm				
	0.5	0.4	0.3	0.2	0.1
	Maximum Principal Stresses, MPa				
250	13.23	13.61	14.72	15.83	20.82
500	26.47	27.21	29.43	31.66	41.63
750	39.7	40.82	44.15	47.49	62.45
1000	52.93	54.42	58.87	63.32	83.26
1250	66.17	68.03	73.59	79.15	104.07
1500	79.4	81.63	88.30	94.98	124.89

Table A- 5 Experimental Validation for Misalgined ASTM Welded specimen

	Maximum Principal Stresses, MPa		
Force, N	Experimental	FEM	% of Differences
250	13.36	11.00	17.64
500	23.70	22.01	7.13
750	34.62	33.01	4.64
1000	45.39	44.02	3.02
1250	58.68	55.02	6.23
1500	68.06	66.03	2.99